X-Ray Diffraction and Adsorption Isotherm Studies of the Calcium Montmorillonite-H_2O System

DONALD SENICH, Major, U.S. Army, Corps of Engineers, and
TURGUT DEMIREL and R. L. HANDY,
Respectively, Associate Professor and Professor, Department of Civil Engineering, Iowa State University

Adsorption isotherm and X-ray diffraction techniques were used to study the adsorption of water on a homoionic calcium montmorillonite at 25 C. The basal d spacings of the primary and secondary reflections, their intensities and line breadth variations were determined in a specially constructed X-ray adsorption chamber. The first-order basal spacing was found to change in a continuous but nonuniform manner. The intensity of secondary reflections was explained on the basis of layer electron density distribution. A comparison of the line breadth, intensity and adsorption data indicates an ice-like configuration of interlayer adsorbed water in the p/p_o range above 0.95. Prolonged X-radiation caused a discoloration of samples attributed to radiation-induced color centers.

Two successive adsorption and desorption isotherms of water vapor on a montmorillonite powder compressed at 25 kg/cm^2 were determined using an electrobalance and an automatic recording device. The isotherms exhibited a hysteresis but were completely reversible in the relative vapor pressure range from zero to 0.20. The rate of adsorption was greater than rate of desorption.

The Langmuir monomolecular model for the adsorption process and the BET multimolecular model were compared, and the latter was found to more closely fit the adsorption data. The BET equation was found to be applicable in the relative pressure range from $p/p_o = 0.11$ to $p/p_o = 0.27$. The specific surface and heat of adsorption of the first monolayer were calculated from the BET parameters.

The adsorption isotherms were used to calculate the free energy changes on adsorption. The free energy changes on successive adsorption cycles compared favorably with loose powder data, indicating that compression had little effect on the magnitude of the free energy change. The free energy changes were divided into two components; one for adsorption on internal surfaces and one for adsorption on external surfaces. Using the data, expansion energies and swelling pressures exerted by calcium montmorillonite were calculated.

•THE phenomena of clay-water interaction are of great interest in such fields as the ceramic and petroleum industries. In soil mechanics, clay-water suspensions have

Paper sponsored by Committee on Physico-Chemical Phenomena in Soils and presented at the 46th Annual Meeting.

been extensively investigated in relation to strength, load-bearing capacity, swelling and shrinkage, and consolidation. However, the direct application of the colloidal principles of surface chemistry has not progressed sufficiently to give the engineer much aid in his interpretations of various curious behaviors observed in clay materials.

It has been generally accepted that clay strength relates to the water films surrounding the individual grains (42). The amount of water normally associated with cohesive soils is characterized by the associated cation and the type of clay mineral. Water can be held rigidly to the surface as surface film water, or in the case of expanding minerals, to internal surface as interlaminar water. When the associated surface films are so thick as to allow individual or groups of particles to slip past each other, the cohesive attraction is reduced. If, however, the water is removed as by evaporation, the surface tension forces at the air-water interface are increased and the water becomes more viscous until such a time as only solid or highly viscous water remains, effectively cementing particles together (33, 41).

The objectives of this investigation were to obtain a complete adsorption-desorption water vapor isotherm, and to obtain analogous X-ray diffraction data during adsorption and desorption of water on calcium montmorillonite; to determine the surface free energy changes during adsorption, expansion energies and swelling pressures; and, by applying the BET theory and other accepted adsorption models, if possible, suggest possible mechanisms of adsorption.

MATERIALS

The clay selected was a commercially available Wyoming bentonite (Volclay-SPV), a product of the American Colloid Company. The sample was purified from coarse-grained impurities by sedimentation, and homoionic calcium montmorillonite was prepared by leaching the fines with a calcium chloride solution. The clay was then washed free of electrolyte as indicated by a silver nitrate test.

METHODS OF INVESTIGATION

X-Ray Diffraction Study

The relative vapor pressure of water made available to the clay sample was continuously controlled by conducting all X-ray tests inside a sealed and evacuated adsorption chamber. The adsorption chamber consisted of a Rigaku-Denki controlled

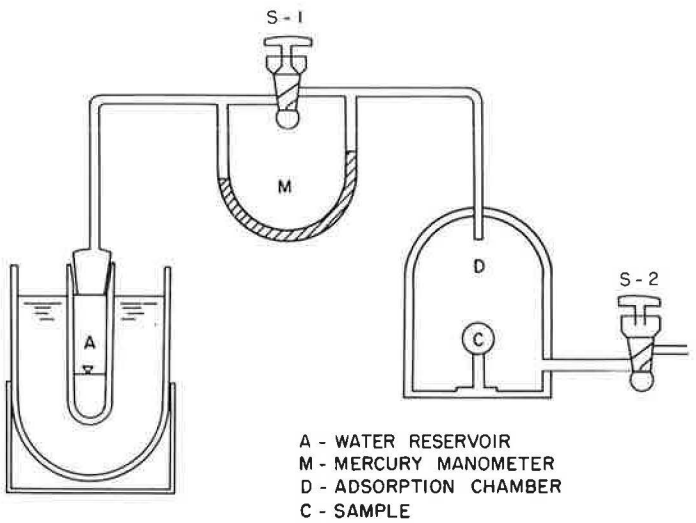

Figure 1. Schematic drawing of X-ray adsorption apparatus.

atmosphere high-temperature X-ray diffractometer furnace modified for use at room temperature (Fig. 1). Heating elements were removed, and the chamber was equipped with a sealed water reservoir separated from the chamber by a mercury-sealed ground glass stopcock and a dual limb mercury manometer. The temperature of the chamber and water reservoir was maintained at 25.0 C.

Water was introduced into the adsorption chamber by means of the mercury-sealed stopcock connecting the water reservoir to the chamber. A cathetometer capable of reading to 0.02 mm was used in measuring vapor pressure differences with the manometer.

X-ray windows on the adsorption chamber were 0.02-mm thick aluminum foil backed with ½ mil "Mylar" polyester film to prevent pinhole corrosion of the aluminum foil by water. A General Electric XRD-5 diffractometer with copper Kα radiation was utilized throughout the investigation. This apparatus is described in detail elsewhere (43, 44).

Approximately 1 gm of prepared clay sample was dispersed in 250 ml of distilled water and deposited in a thin layer on a 30-mm diameter medium-porosity fritted glass disc, by draining the suspension through the disc using a water aspirator. After one day of air-drying and five days drying over phosphorous pentoxide, the sample was placed in the adsorption chamber and the top of the chamber was clamped tightly in place. All joints were lubricated with high-vacuum grease to eliminate leaks. Triple-distilled water was placed in the water reservoir, dipped into a dry ice-aceton mixture and the system was evacuated using a mechanical fore pump and an oil diffusion pump. The system was pumped for 26 days; vacuum was maintained at 5×10^{-5} mm Hg, indicated by an ionization gage, for the last eight days. The water in the reservoir was frozen and thawed five times for degassing.

The chamber was then removed from the pump and aligned on the X-ray diffractometer. As soon as thermal equilibrium was attained the collapsed 001 basal spacings were measured by X-ray diffraction. Immediately thereafter, a small increment of water vapor was distilled into the adsorption chamber and X-ray tests were made periodically up to 24 hours, which was the minimum allowed for the system to reach equilibrium after a transfer of water vapor. This procedure was repeated until saturation was reached.

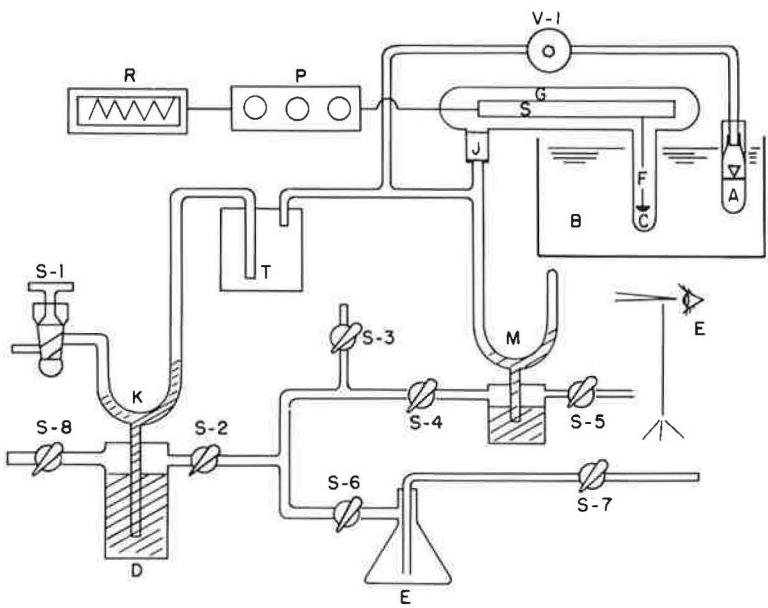

Figure 2. Adsorption isotherm apparatus.

A gradual desorption was then accomplished by redistilling water back into the water reservoir by employing a cold bath around the reservoir, with equilibration and test procedures performed as before.

X-ray diffraction intensities were obtained from measurements of diffraction peak areas with a planimeter. At least three peaks were averaged.

Sorption Isotherm Study

The adsorption and desorption isotherms were determined gravimetrically. The adsorption apparatus (Figs. 2 and 3) consisted of an electrobalance system comprised of a beam balance (S), control unit (P), and vacuum flask (G), connected to a Sargent model SR recorder (R). The electrobalance was connected to the vacuum train by means of a large ground glass stopcock (S-1) and a mercury dual-limb cutoff (K). The sample (C), suspended from the electrobalance in a hang-down tube (F), and a mercury sealed water reservoir (A), were both suspended in a constant-temperature bath (B) having a capacity of 16 liters. The constant-temperature bath was equipped with a tap water cooling coil, a Beckman thermometer reading to 0.01 C, a continuous heater, and an intermittent heater mercury regulator relay circuit. The immersed heaters were two 100-watt light bulbs with variable transformer voltage control. Room temperature was maintained at about 2 C above that of the thermostat. Temperature variation in the thermostat (B) was not more than plus or minus 0.02 C throughout the entire investigation.

The tube A was the water reservoir used for introducing water into the system, and was attached to the system by means of an ultrahigh vacuum valve (V-1). M is a simple mercury manometer used to determine the pressure in the adsorption chamber. The level of the mercury in the manometer was maintained by use of a mercury reservoir, the water aspirator and stopcocks (S-4 and S-5). D is a mercury reservoir used to supply the cutoff K, stopcocks S-2 and S-8 being used to control the level of the mercury in the cutoff. A cold trap (T) was used during degassing to trap mercury vapor in the system. Stopcocks (S-2, S-4, and S-6) isolated the system from the water aspirator. All glass parts in the system were Pyrex, and a high-vacuum silicone grease was used for all joints.

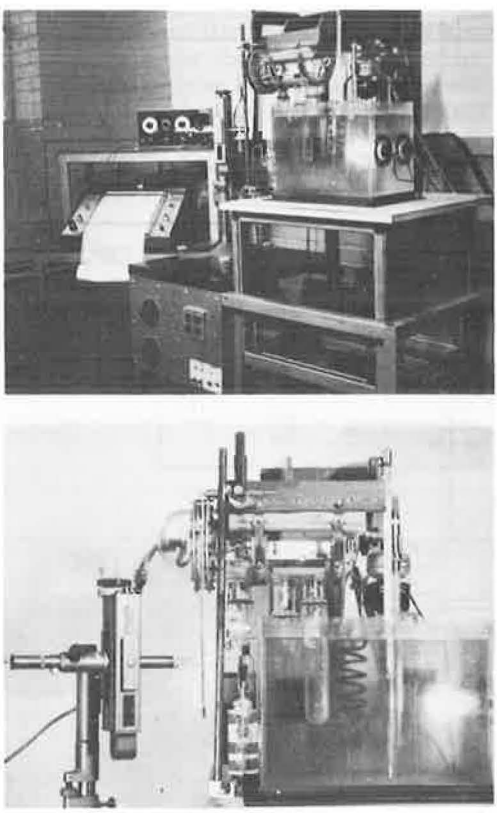

Figure 3. Adsorption isotherm apparatus.

A cathetometer (E) used to read the manometer (M) was rigidly mounted on a soapstone table top tied to a steel framework to eliminate any movement during unattended periods. The electrobalance was affixed to a ten-inch steel pipe which extended through the floor and was embedded at the bottom in several feet of chipped hard rubber to eliminate room vibrations. The load capacity of the balance is 1.0 gm. The smallest weight that could be reliably detected was 10^{-6} gm. Changes in the sample weight cause the beam S to deflect momentarily; this motion changes the phototube current which is amplified and applied to the coil attached to the beam. The coil is in a magnetic field, so the current passing through it exerts a moment on the beam, restoring

it to balance. The current is an exact measure of the sample weight. A signal is sent to the control unit P where it is amplified and the final signal is fed to the automatic recorder R.

Attached to the electrobalance is a cadmium trap (J) whereby small strips of cadmium were placed in this well to trap any mercury vapor from the manometer.

A sample containing 305 mg of calcium montmorillonite was placed in a stainless steel ring (ID 0.375 in.) and then equilibrated under a bell jar containing hot water for two hours. The loose sample and the ring were removed from the bell jar and placed on a press where the sample was subjected to a load of 25 kg/cm^2 for two hours. After removal of the load, the sample was allowed to air-dry for one day. Freshly boiled, triple-distilled water was introduced into the reservoir A; the reservoir was attached to the adsorption chamber and the pill-shaped sample was placed on the electrobalance pan in the hang-down tube of the electrobalance. After evacuating the system with the water aspirator, the sample was connected to the high-vacuum train and the system was pumped for 37 days with the mechanical and oil diffusion pumps. Degassing of the water in the reservoir to release its trapped gases was repeated five times utilizing a dry ice-acetone mixture.

After 37 days of pumping, the weight of the sample and the pressure on the vacuum gage were 265.05 mg and 4×10^{-5} mm Hg, respectively. Manometer readings were taken as soon as the evacuation was completed, and after correcting for temperature, gravity, and meniscus depression, the pressure was found to be 0.00 mm Hg. Immediately after taking the manometer readings, a reading of the automatic recording device was made to determine the equilibrium weight in milligrams.

Valve V-1 was opened slightly to allow a small increment of water vapor to enter the adsorption chamber. Valve V-1 was then closed and the weight automatically recorded on the apparatus as adsorption proceeded on the sample. Very small increments of water vapor were introduced in order to obtain the maximum number of points during adsorption. In this manner, more and more vapor was introduced into the adsorption chamber and the pressures up to saturation at constant temperature were investigated.

In the vicinity of saturation the high-vacuum valve V-1 was left open and after there was no additional rise in weight of the sample, a small amount of ice water was introduced against the side of the hang-down tube (F) containing the sample. This produced a small amount of dew on the tube, and the time for the dew to disappear was observed. At pressures below saturation the dew disappeared rapidly, whereas at saturation the time of disappearance sharply increased. The weight as recorded on the automatic recorder showed very little change in the weight of the sample while the dew persisted on the side of the chamber.

The desorption isotherms were obtained by condensing more and more vapor back into the water reservoir by cooling it with ice water. The sample was pumped with the vacuum train at relative pressure, p/p_o, below 0.3.

DISCUSSION AND PRESENTATION OF RESULTS

X-Ray Data

The accuracy in determination of X-ray diffraction peak positions depended on the angle at which the peak position appeared, the relative sharpness of the peak, the accuracy in alignment of the sample, and the alignment of the instrument. The alignment of the instrument and the effect of systematic errors were tested by X-raying an EDDT crystal and an ADP crystal. It was determined that the values in d_{001} position were within ±0.003 Å of published data; therefore, no correction was necessary. During the investigation a standard deviation, σ, for the sample d_{001} was evaluated and found to be ±0.03 Å at 9 deg 2θ and ±0.10 Å at 5 deg 2θ. For measured line breadths of the diffraction peaks obtained were taken as the peak width at half-maximum intensity (28). The intensities shown in Figure 4 were measured by planimetering the diffraction patterns and then were corrected for the Lorentz-polarization factor by use of the international tables for X-ray crystallography (26, p. 270) and expressed relative to the starting intensities.

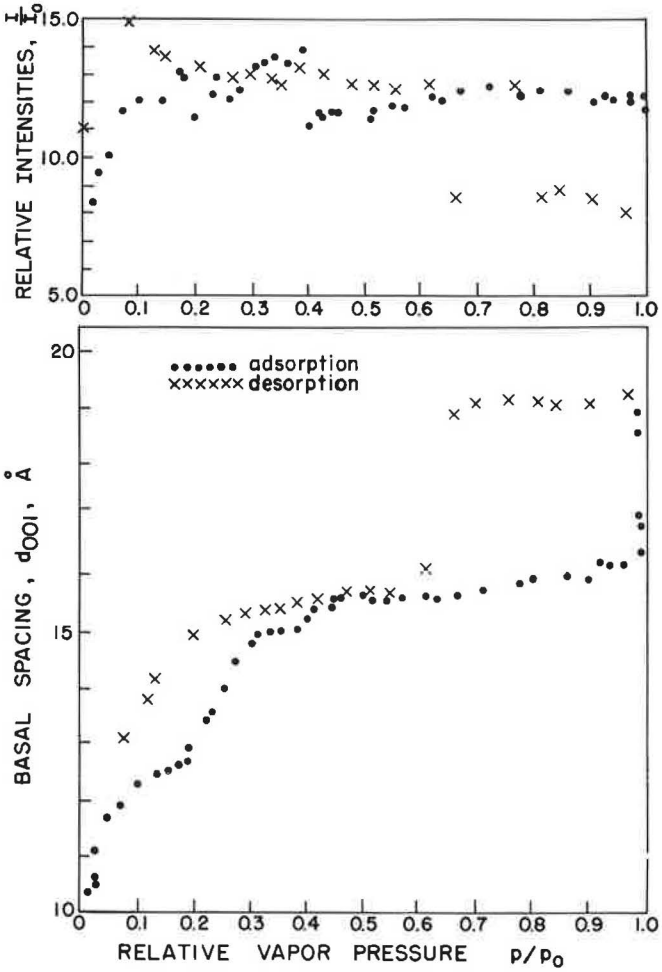

Figure 4. Variations in the first-order basal spacings and relative intensities vs relative vapor pressure for calcium montmorillonite.

Figures 4 and 5 are plots of the apparent first-order basal spacings vs the relative vapor pressure at which they were observed. The upper plots are the line breadths and intensities, respectively, vs the selected relative vapor pressures, expressed relative to the reference line breadth and intensity observed prior to the introduction of water vapor into the system.

As can be seen from the curves, the changes in average basal spacing take place in a continuous but nonuniform manner with changes in relative vapor pressure. Hendricks and Jefferson (23) hypothesized that the X-ray diffraction patterns from an expanding powder should show that the basal spacing would vary continuously with water content. As the relative vapor pressure is increased from zero, there is a slight increase in d spacing up to $p/p_0 = 0.015$. This would seem to indicate that only a small portion of vapor is adsorbed in the interlayer region, while the rest is adsorbed on the external surfaces. The expansion then rapidly increases to 11.9 Å between $p/p_0 = 0.015$ and $p/p_0 = 0.08$, indicating an expansion equivalent to one molecular layer of water when 1.8 molecules per unit cell are adsorbed. There is a small hump in the curve between $p/p_0 = 0.08$ and $p/p_0 = 0.11$, perhaps associated with the space occupied by a calcium cation. The d spacing is stable from $p/p_0 = 0.11$ to $p/p_0 = 0.19$;

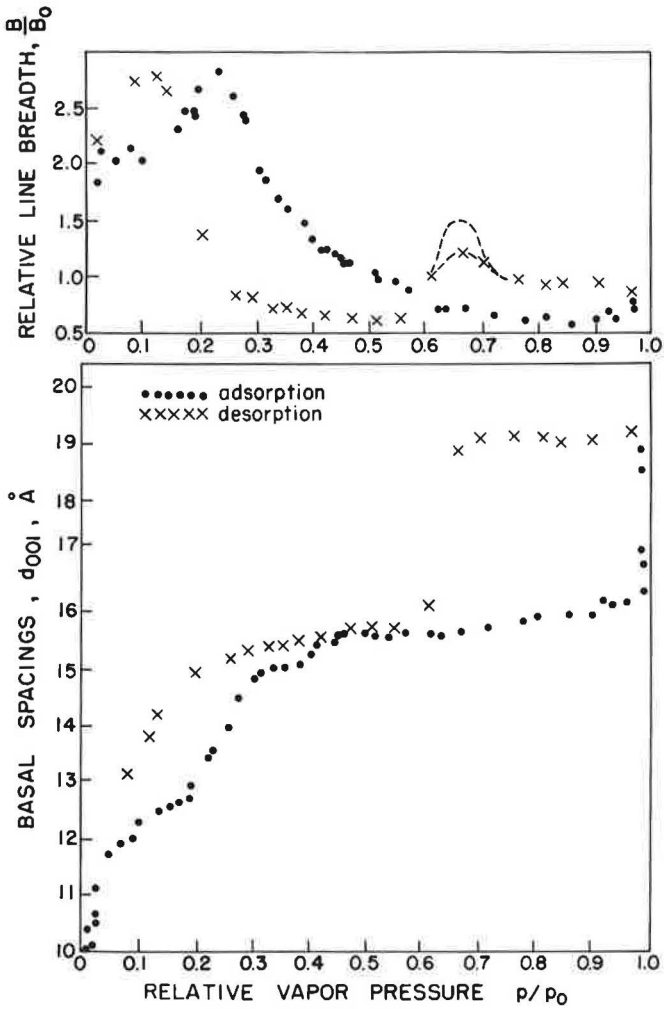

Figure 5. Variations in the first-order basal spacings and line breadths vs vapor pressure for calcium montmorillonite.

then the second major expansion from 12.6 Å to 15.1 Å occurs between p/p_0 = 0.19 and p/p_0 = 0.30 with the uptake of 5.5 molecules per unit cell.

There is a second hump in the curve between p/p_0 = 0.38 and p/p_0 = 0.42, perhaps associated with the coordination of molecules of water with the cation. The total uptake of water necessary to attain the stable 15.6 Å configuration is 7.5 molecules per unit cell. Between p/p_0 = 0.42 and p/p_0 = 0.98, there is a stable range of d spacing where the spacing increases only 0.8 Å while adsorbing 12 molecules of water per unit cell. The final increment of expansion occurred between a relative vapor pressure p/p_0 of 0.99 and saturation. This final expansion to 19.26 Å requires the adsorption of approximately 14 molecules per unit cell and required 242 hours to attain equilibrium. The 19.26 Å was the maximum spacing that could be obtained with this interlayer cation (34).

The desorption curve experienced two hysteresis loops, the first occurring between saturation and p/p_0 = 0.60, and the second, which is less pronounced, between p/p_0 = 0.3 and zero.

The effect of time and pressure gradient were evident in the final expansion during adsorption and in the first collapse during desorption. The pressure gradient for the

last expansion was very small (0.24 mm), corresponding to p/p_o = 0.99 to p/p_o = 1.00, and full expansion took place after 242 hours. Prior to this point, all expansion had been completed almost immediately after introduction of each increment of water vapor. The equilibrium pressures and peak positions were determined after 24 hours, although the expansion had been completed within the first 30 minutes. During desorption, all collapse was completed after no more than 16 hours. The first collapse of the platelet system took place between p/p_o = 0.65 and p/p_o = 0.60, but the desorption curve did not return to the original d spacing. This suggests that interlayer water was trapped in the pores or remained associated with the cation. A pumping period of ten days utilizing a dry ice-acetone bath surrounding the water reservoir produced a shift from 11.5 Å to 10.7 Å, but the relative line breadth increased as water was removed, indicating a disordered system. It is reasonable to visualize that the isolated water islands are well within the platelet structure, their exit being blocked or impeded as the clay surfaces on each side of the islands move more closely together.

The plot of the X-ray line breadth vs relative vapor pressure (Fig. 5) tends to substantiate the conclusion that there are varying numbers of molecular interlayers, i.e., 0, 1, 2, etc., and that an octahedral coordination of water around the cation may exist within the interlaminar spaces. Between a relative vapor pressure of zero and p/p_o = 0.08, the line breadth increases corresponding to an uptake of water, indicating non-uniform spacing in the interlayer regions. We may note that line breadth reaches a maximum near the center of the steeper portions of the basal spacing plot, and then decreases to a minimum value or remains constant as the basal spacing plot approaches flatter sections. A low value of line breadth is indicative of a uniform spacing (10).

When d_{001} was between 10.5 Å and 15 Å, a broad peak appeared at approximately twice the d_{001}, indicating a possible repeating double layer structure (superlattice) including water molecules. The clean porous disc on which the clay sample was deposited had been tested using copper radiation, and gave a typical amorphous pattern expected from a glassy material with no indication of the peaks obtained with the calcium montmorillonite sample. A superlattice has been reported by Brindley (8, p. 151) for chlorites, Brindley (9, pp. 93-96) for serpentine, and Gillery (22) and Demirel (16) for calcium montmorillonite. Demirel suggests that the offset stacking of platelets to match the water molecules with oxygen atoms of the silica surfaces must repeat in an organized manner in the c direction. Gillery attributes the diffuse band to a two-layer natural stacking of the layers which may be due to a tendency to form two types of montmorillonite lattices which alternate, or hydration tending to take place in alternate layers. Using copper radiation and the beam slit-detector slit configuration in this investigation, the diffuse band could not be clearly resolved.

Comparison With Work of Other Investigators

Nagelschmidt (37) dried calcium montmorillonite samples in a furnace at temperatures between 85 C and 245 C, rehydrated them over salt solutions, sealed them in capillaries of 0.77-mm internal diameter, and took X-ray photographs. He noted a proportional increase in the basal spacing from 10.5 Å to 15 Å during the uptake of the first four molecules of water per unit cell, and an increase of 0.6 Å during the uptake of the next ten molecules of water. He explained that the small increase in d spacing was due to the adsorption only on the external surfaces.

Mooney et al (35, 36) used a Wyoming bentonite, Volclay-SPV, and prepared a homoionic calcium montmorillonite from this bentonite. In a plot of d spacing vs relative vapor pressure, they found that the spacing leveled off between 12 Å and 13 Å and between 15 Å and 16 Å, which values corresponded to integral numbers of layers of water molecules between platelets. They obtained a spacing of 16.5 Å, which was apparently ignored in their conclusions, but were not able to obtain a 19 Å spacing, perhaps due to insufficient hydration. They reported no hysteresis in their curves although they apparently completed their adsorption cycle at a relative vapor pressure of approximately 0.90. In the present study, the last platelet separation occurred between p/p_o = 0.98 and saturation; the present data indicate that if Mooney et al (35, 36) actually began their desorption at p/p_o = 0.90 and the second desorption equilibrium

pressure point was lower than $p/p_o = 0.60$, no hysteresis would have been observed. These data illustrate the importance of obtaining complete evacuation of the system prior to adsorption, and complete adsorption to saturation prior to desorption.

Gillery (22) used a natural Wyoming bentonite supplied by the National Lead Company. After running adsorption studies on sodium montmorillonite, he resaturated the material with $CaCl_2$ obtaining a homoionic calcium montmorillonite. The relative humidity was controlled by passing compressed air through appropriate saturated salt solutions and into the sample chamber; humidities were measured with wet and dry thermocouples. The sample was investigated during the desorption phase. Gillery states that the plot of basal spacing vs percent relative humidity suggests a mixture of sodium and calcium cations. He suggests that the adsorbed cation affects the characteristics of adsorbed water by showing hydrates of 12.3 Å over a very small stability range of about 5 percent relative humidity, while the second hydrate of 15.5 Å has a stability range from about 35 percent relative humidity to saturation. He suggests that a hydrate of 18 Å exists, but that $p/p_o = 1.00$ is not sufficient water vapor pressure to produce this hydrate in a pure form, and the final hydrates exist only in a mixed layer form with the 15.5 Å hydrate. The present study indicates that if sufficient time is allowed for hydration, the 19.2 Å hydrate can be obtained.

Hendricks et al (24) used montmorillonites from California, Mississippi and Wyoming saturated with various cations. Their material was equilibrated over salt solutions and the samples selected for X-ray investigation were sealed in glass capillary

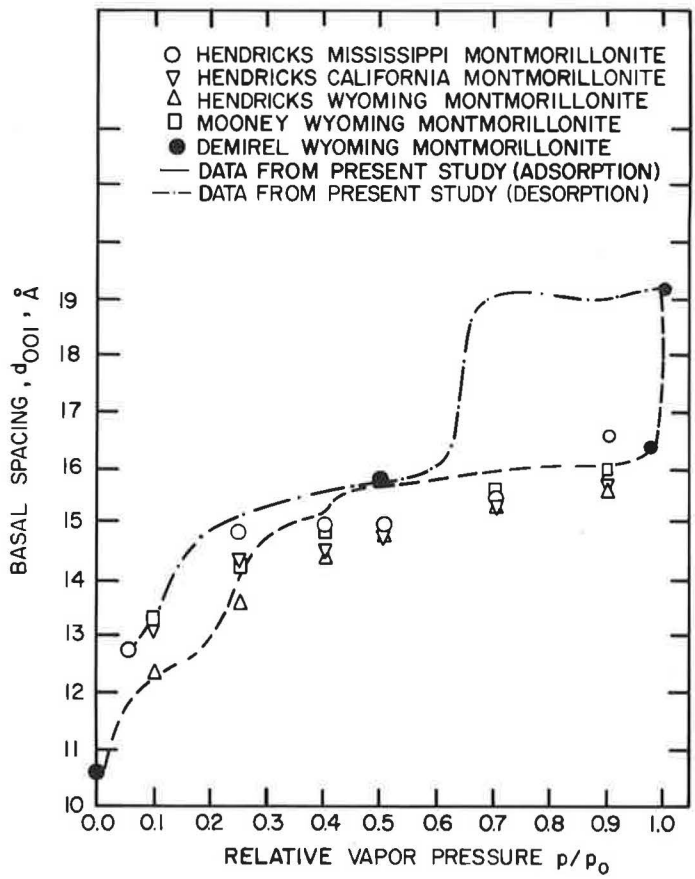

Figure 6. Variations in the first-order spacings vs relative vapor pressure for calcium montmorillonites reported by various authors.

tubes to prevent loss of water. The samples were placed in X-ray cameras for diffraction measurements for periods of 10 to 48 hours. There was considerable scatter in the data. The relative humidities reported were those determined while the samples were in the adsorption chamber or desiccator. No reference was made to any method for temperature control, which may account for the scatter.

Demirel (16) equilibrated his dry samples at room temperature in vacuum desiccators maintained at the desired relative humidities by appropriate salt solutions. A Plexiglas hood equipped with a Mylar X-ray window covered the sample and salt solution during X-ray studies. Although only four points were obtained for adsorption, Demirel was able to attain full expansion at saturation by immersing his sample in distilled water.

The data of these various investigators are shown in Figure 6 for comparison with the present study.

Color Changes During Irradiation

Upon completion of the X-ray studies, the sample had been under copper irradiation for approximately 1,000 hours. When it was removed from the apparatus, a very distinct color change was evident; whereas the sample had been a yellowish white prior to testing, it was a dark greenish blue after irradiation. Normal chemical tests and fluorescent analysis were performed to determine if some impurities may have been in the sample.

The fluorescent analysis was run using tungsten radiation with LiF, NaCl, and EDDT analyzing crystals on four different specimens: (a) the 1,000-hour irradiated sample; (b) a sample that had been evacuated to 10^{-5} mm Hg for 20 days and irradiated with copper radiation for 26 hours; (c) an air-dried sample of calcium montmorillonite; and (d) a plain fritted porous disc similar to that used in the sample holder of the apparatus.

The fluorescent diagrams showed small traces of tungsten and iron; the tungsten was attributed to tungsten used in the manufacture of the porous disc or more likely from the tungsten X-ray tube, and the iron peaks in all three clay samples were of the same magnitude of intensity and can be attributed to the iron substitution in the octahedral layer (isomorphous substitution).

The possibility of mercury contamination was eliminated for two reasons: (a) no traces of mercury were found during fluorescent analysis; and (b) the clay specimen in the electrobalance was exposed to a greater surface area of mercury in the limbs of the manometer attached to the electrobalance with no discoloration than the surface of the limbs of the manometer attached to the X-ray apparatus.

Therefore, the discoloration can be due to (a) a change in the valence state of a naturally occurring metallic impurity in the host crystal (e.g., Fe in MgO is a known example of this); or (b) a radiation-induced color center in the crystal (e.g., electron trapped at a halogen ion vacancy in an alkali halide). In either case, about ten ppm could produce the observed effect.

Diffraction Intensity

The structure factor is a complex quantity whose magnitude is the amplitude of the scattered wave, and whose direction is determined by the phase of the scattered wave. No matter how complicated a crystal, one may picture it as a series of simple interpenetrating simple lattices, one for each different atom in the crystal. The problem of evaluating the structure factor can be considered to be that of compounding several wave motions, all of the same period, but different in phase and amplitude.

Other factors also affect diffraction intensity:

$$I = \theta \left| F_{\ell} \right|^2 \Psi \qquad (1)$$

where θ is the combined Lorentz-polarization factor, F_{ℓ} is the layer structure factor, and Ψ is the mixing function. The Lorentz-polarization factor depends in part on

experimental technique, and may be estimated from the international tables for X-ray crystallography (26). Importance of the Lorentz-polarization factor at low diffraction angles is illustrated by the fact that it will cause a 17 Å peak to be three times as intense as a 10 Å peak, other factors being the same.

The mixing function Ψ depends on the spacings of the constituent phases and the frequency of the occurrence of these spacings. When a montmorillonite system becomes ordered (the system is made up of nearly all one primary spacing), the intensity will increase, whereas if there were many spacings present, the intensity of reflections will decrease.

By taking the center of the silicate layer as the plane of the origin and limiting the analysis to basal (00ℓ) spacings, the structure factor reduces to

$$F_{00\ell} = 2 \sum_{j=1}^{J/2} f_j \cos 2\pi (\ell z_j) \qquad (2)$$

(13, p. 264), where f_j is the structure factor of the j th atomic layer, ℓ is the Miller index, and z_j is the fractional position of each reflecting layer in the unit cell.

The minimum d_{001} spacing of 10.1 Å was observed at zero relative pressure. This distance corresponds to the 9.2 Å thickness of the pyrophyllite silicate structure, with layers separated by calcium ions fitting with a coordination of six between opposing silica tetrahedra bases. The maximum basal spacing observed was 19.2 Å, occurring at saturation.

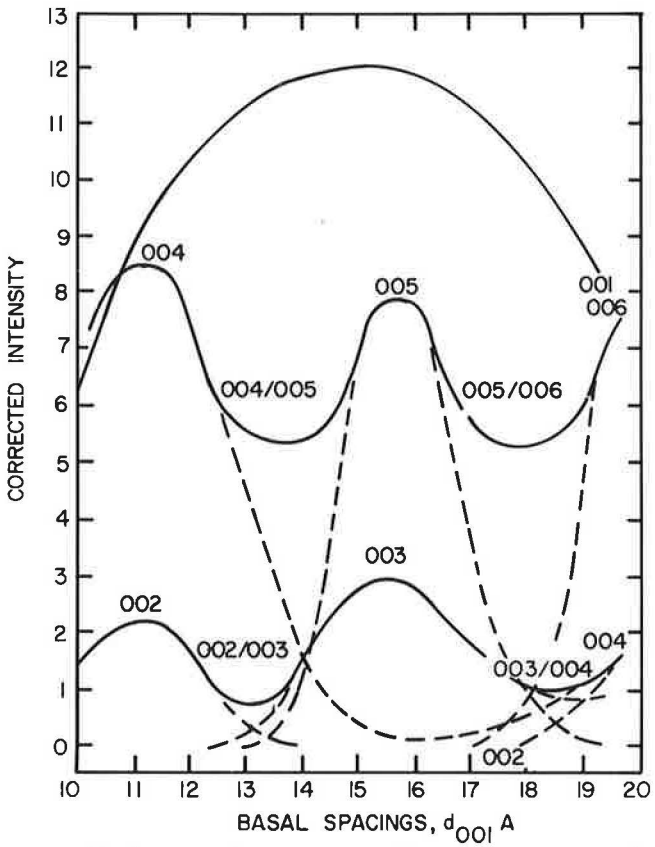

Figure 7. Intensity of higher order basal spacing reflections vs first-order basal spacing.

Intensities of the first- through sixth-order basal spacings corrected for the Lorentz-polarization factor are shown by the solid lines in Figure 7. Nearly always the first order reflection d_{001} was the most intense; its intensity reaching a maximum at intermediate d spacings. On the other hand, d_{002} reflections were observed only at high and at low d spacings. This same observation applies to other higher order spacings: odd-numbered indices gave strongest reflections in the intermediate range of d spacings, and even-numbered indices gave strongest reflections at high and low d spacings.

For d spacings between those which give maximum intensities, e.g., in the range between 004 and 005 maxima, line breadths and d spacings suggest that the observed reflections are composites of two indices, in this case 004/005. Based on this interpretation, individual intensity maxima may be resolved into the contributing components, indicated by dashed lines in Figure 7.

The absence of diffraction peaks qualitatively indicates the presence of repeating electron density planes at the d/2 spacing. That is, if d gives a diffraction due to waves being one wavelength out of phase, a plane of atoms occurring at d/2 will produce waves one-half wavelength out of phase, and the result will be annulment. This may be seen by Eq. 2, where z_j indicates the vertical positions of atoms in the unit cell. In this case the structure factor equals $2[f_1 \cos 2\pi (1) + f_2 \cos 2\pi (1/2)]$, or if f_1 and f_2 are equal, $2[f - f] = 0$.

Referring to Figure 7, extinction of the 002 when d_{001} is between 13 and 18 Å indicates a layer of atoms in the region 3.2 to 4.5 Å outward from the center of the clay layer (Table 1). In the pyrophyllite structure this approximately corresponds to the outer layers of oxygen atoms.

Similarly, the lack of 003 for d_{001} of 18 to 20 Å may relate to position of the silicon layers, and extinctions of the 005 and 006 appear to relate to position of the O + OH layers. The 003, 004, and 005 extinctions also indicate a layer of atoms at about 2 Å from the aluminum layer; this is unexplained, and may be due to other factors.

This study was undertaken mainly to determine structure, if any, of the interlayer water and position of the cations. In this connection the d_{001} intensities were lowest when diffraction lines were sharpest and spacings were presumably most uniform. This occurred at zero relative pressure and near saturation, when d_{001} was 10.1 and 19.2 Å, respectively. As shown in Table 1, in these particular cases the structure factor suggests planes of atoms occurring approximately midway in the interlayer region. Presumably these are the exchangeable calciums.

Possible Configuration of Interlayer Water

Hendricks and Jefferson (23) have suggested that because of the dipole character of the water as well as the lattice characteristics of the clay mineral surface, water molecules are joined by hydrogen bonding into groups of extended hexagonal networks. By assuming a 3.0 Å separation of oxygen, such a water network has a and b dimensions of the clay minerals, and every other water molecule in the net has one hydrogen available for bonding to an oxygen of the clay mineral surface. Successive hexagonal nets build up on one another and are hydrogen-bonded to one another. This hypothesis leads to a laminar stacking of a hexagonal water molecule network with a vertical separation of 2.76 Å for each layer. In this configuration each water molecule in a monomolecular layer occupies an area of about 11.5 $Å^2$ (16).

TABLE 1

INFERRED POSITION (z) OF ATOMIC LAYERS RELATIVE TO THE CENTRAL Al LAYER

00ℓ	d_{001} at $d_{00\ell}$ Annulment	$Z = \frac{d_{00\ell}}{2}$	Probable Layer Identifications
001	10.1 (weak)	5	Interlayer Ca
	19.2 (weak)	9.6	Interlayer Ca and water
002	13-18	3.2-4.5	Outermost O layer
003	10-13	1.7-2.2	?
	18-20 (weak)	3-3.3	Silicon
004	14-18	1.7-2.3	?
005	10-14	1-1.4	O-OH layer
	18-20	1.8-2.0	?
006	10-18	0.9-1.5	O-OH layer

Macey (29) pointed out that there is a similarity between the basal plane of ice and the oxygen layer of the basal plane of clay mineral. In the clay interlayer oxygen surface, the oxygen atoms are 4.51 Å apart, whereas the oxygens of the basal plane of ice are 4.52 Å apart. Assuming an ice configuration, there are $2^2/_3$ mole-

cules of water per unit cell, and each water molecule covers an area of about 17.5 $Å^2$ (16). Macey suggests that the ice structure develops on clay mineral surfaces with the hexagonal molecular configuration of the basal plane of ice and tends to build outward from the surface. This configuration was supported by Forslind (19) using the Edelman-Favejee clay lattice structure.

Barshad (4) has postulated various configurations for the water molecules adsorbed. He suggests that for a monomolecular layer of water the maximum expansion would be 2.76 Å if the centers of the oxygens of the water molecules were vertically above the centers of oxygens in the basal plane of clay mineral lattice, whereas the separation would be only 1.78 Å if the water molecules form tetrahedra with the bases of the linked silica tetrahedra of the clay mineral lattice. Three possible arrangements may occur depending on the manner of superposition of one monolayer of water on the other. If the water molecules form tetrahedra at the water-oxygen interface and octahedra at the water-water interface, the arrangement would give a separation 3.87 Å. If the water molecules form tetrahedra at the oxygen-water interface but are vertically above each other at the water-water interface, this would give an octahedral arrangement with a separation of 4.54 Å. If the water molecules are vertically above and below the oxygens of the clay surface and are also above each other at the water-water interface, the arrangement would give a thickness of 5.52 Å.

When three monomolecular layers are present, three possible separations are 5.96 Å, 7.30 Å, and 8.28 Å, respectively. Depending on the arrangement at the clay surface, the area covered per molecule may be about 11.5 $Å^2$ or 7.7 $Å^2$.

The results of Demirel's studies (16) suggest that water is adsorbed in the interlayer regions in the form of ice-like structure. This agrees essentially with Macey's hypothesis that a stacking of the hexagonal rings occurs in the quartz-like structure of ice: the first and second layers form a separation of 2.76 Å each; the third and fourth layers fill in between the hexagonal networks forming tetrahedrons with the molecules of the network. The complete unit cell of ice is formed with the entrance of the fourth layer, causing a separation of 7.36 Å. The fifth and sixth layers of water enter between the unit cell of ice and the clay surfaces, causing total separation of 10.12 Å and 12.88 Å, respectively. The area occupied by a water molecule in this method is approximately 17.5 $Å^2$.

Opposing this view, Mackenzie (30) questions the validity of an ice-like structure. Nuclear magnetic resonance studies by Wu (49) on montmorillonite at low temperatures do not substantiate the theory of ice structure. He points out that at temperatures below 0 C, the evidence indicates that the water close to the clay has a structure but it is different from that of ice. Wu further points out that selective adsorption sites exist for the first few molecules of adsorbed water, but that the water molecules are not bound to fixed positions but are under considerable thermal agitation.

Roderick (43, 44) gives evidence of the formation of a laminated arrangement of interlayer water rather than an ice-like structure for a sodium montmorillonite with up to three layers of water. Mering (34) performed water vapor adsorption studies on calcium montmorillonite at 30 C and deduced that initially the first stage of hydration is the formation of groups of six H_2O molecules around every cation. He further suggested that the "hydrate" with two layers of water begins to form immediately after the hydration of the cations without passing through a one-layer state.

There are approximately 0.35 calcium cations per unit cell; therefore, a three-unit cell system satisfied by one cation is the basic model that will be utilized. From the data available, the possible uptake and arrangement of the interlayer water molecules are visualized as follows. The first layer of water forms a network shared by two montmorillonite platelets causing a separation of 2.76 Å. At this point approximately two molecules of water per unit cell are adsorbed. After the first two molecules per unit cell are adsorbed, there is a small increase which may be attributed to the space occupied by the calcium ion, and which may be considered as the state in which the first monolayer is completed and the start of the hydration of the cation occurs. The observed spacing may be explained if the water molecules are shared by the cation and are located in positions directly below oxygens of the mineral surface, while the cation is located in the base of the tetrahedron in the hexagonal framework of the mineral surface.

As the second layer of water enters and 5.5 molecules of water per unit cell are adsorbed, two hexagonal networks stacked in a laminar fashion would give the proper amount of water per unit cell and give a d spacing of 14.7 Å. The larger observed spacing 15.1 Å can be attributed to space occupied by the cation. A straight laminar stacking including the cation would have given a spacing of 15.6 Å; it is concluded that the 15.1 Å spacing is an average value from the 14.7 Å and 15.6 Å peaks. This view is supported by the line breadths, which are very broad in this region (Fig. 5).

The 15.6 Å spacing relates to the entrance of additional water, and on the basis of the subsequent structure, this spacing, which also gives a broad peak, may be the start of an ice-like configuration with the formation of tetrahedrons with the water molecules of the hexagonal network. The 15.6 Å spacing is associated with the adsorption of 7.5 molecules of water per unit cell.

A four water-layer ice-like configuration causing a separation of 7.36 Å can be obtained by the adsorption of 12 molecules of water per unit cell, and gives a d spacing of 16.5 Å. The observed combination of minimum line breadth and maximum intensity lends credence to the hypothesis of an ice-like configuration containing least disorder. The cation in this case fits loosely in holes, and does not directly affect the spacing.

Apparently a fifth molecular layer of water enters between the configuration, giving a less ordered structure but causing a minimum line breadth at 19.2 Å. An observed decrease in the intensity of the 001 reflections in the region of saturation must be an indication that the water molecules and/or cations have some structure effect. As the relative vapor pressure increased from p/p_o 0.42 to p/p_o 0.95 the interlaminar water content increased, but there was no significant change in intensity. After p/p_o 0.95, intensity decreased. In general, the effective structure factor may be expressed as a combination of the contribution from the mineral structure plus the effect of the interlayer cations and water molecules. At large separations, the ordering effect of the mineral surface is reduced and there is a buildup of electron population of water and the cations midway between the two sheets. Therefore, the 001 reflection would be reduced because the electron density would be exactly out of phase, although of a much-reduced amplitude. The decreased intensity suggests that the cations may now be centrally located, and prevention of further expansion is by symmetrical ion-dipole linkages between the layers.

As pointed out, the ice-like configuration is completed in a very limited range of relative vapor pressure near saturation. The configuration proposed in this study is not in basic contradiction with the ice structure proposed by Macey (29) and Demirel (16) nor with the nuclear magnetic resonance studies of Wu (49). At the present time there have been no nuclear magnetic resonance studies published concerning work conducted at relative humidities at which the ice-like configuration results. Perhaps future studies can be conducted so as to bring more light upon the interlayer water theories.

Other alternatives for the arrangement of water were also considered. In the case of laminated stacking, a separation of 2.76 Å would be caused by the adsorption of each

TABLE 2

COMPARISON OF OBSERVED FIRST ORDER BASAL SPACINGS OF CALCIUM MONTMORILLONITE WITH THOSE CALCULATED FROM MONTMORILLONITE PLATELET THICKNESS (c_o) AND HYPOTHETICAL MECHANISM OF THE ADSORPTION OF WATER

Number of Molecular Layers of Water	Ice Configuration		Laminated Stacking		Barshad's Alternatives[a]		
	Based on Pyrophyllite Thickness	Based on d_{001} of Collapsed Montmorillonite	Based on Pyrophyllite Thickness	Based on d_{001} of Collapsed Montmorillonite	Alternative 1	Alternative 2	Alternative 3
0	9.14	10.1	9.14	10.1	10.16	10.16	10.16
1	11.90	12.86	11.90	12.86	11.94	12.92	
2	14.66	15.62	14.66	15.62	14.03	14.70	15.68
3	14.66	15.62	17.42	18.38	16.12	17.64	18.44
4	16.50[b]	17.46	20.18	21.14			
5	19.26	20.22	22.94	23.90			
6	22.02	22.98	25.70	26.66			

[a]Based on a minimum d spacing of 10.16 as proposed by Barshad (4).
[b]Corresponds to a single-unit cell of ice-like structure between platelets.

additional molecular layer of water. Table 2 indicates that the ice configuration explains the data in a better manner than does the laminated stacking concept.

The hypothesis proposed by Barshad (4) for the configuration of the interlaminar water was also examined, and the spacings proposed by him are included in Table 2. As can be seen, these values can be utilized if one uses all three of his alternatives simultaneously. However, the configuration would be changed for each increment of water layers that entered. For example, alternative No. 1 could be used to explain the system with zero and one layer of water. Alternative No. 2 could be used to explain the system with zero, one, and two layers. Alternative No. 3 could be utilized to explain the system with two layers of water only. The arrangement proposed in the preceding discussion, i.e., a buildup of water in an ice-like configuration, appears to more aptly describe the observed spacings.

SORPTION DATA

Figure 8 is a plot of the adsorption and desorption isotherms for the first and second cycles. The desorption branch for the first and second cycles did not return to the initial value of q = 0. For the entire range of the adsorption and desorption isotherms, the final point showed differences of 0.3 percent and 0.25 percent in the first and second desorption runs, respectively. These differences may or may not be real, since readings of the calibrated dial on the automatic recording device or marking pen position may have introduced an error. However, if this difference is real it may be attributed to trace amounts of individual or clustered water molecules that were trapped within the interlayer positions if the pumping period were insufficient in length to re-

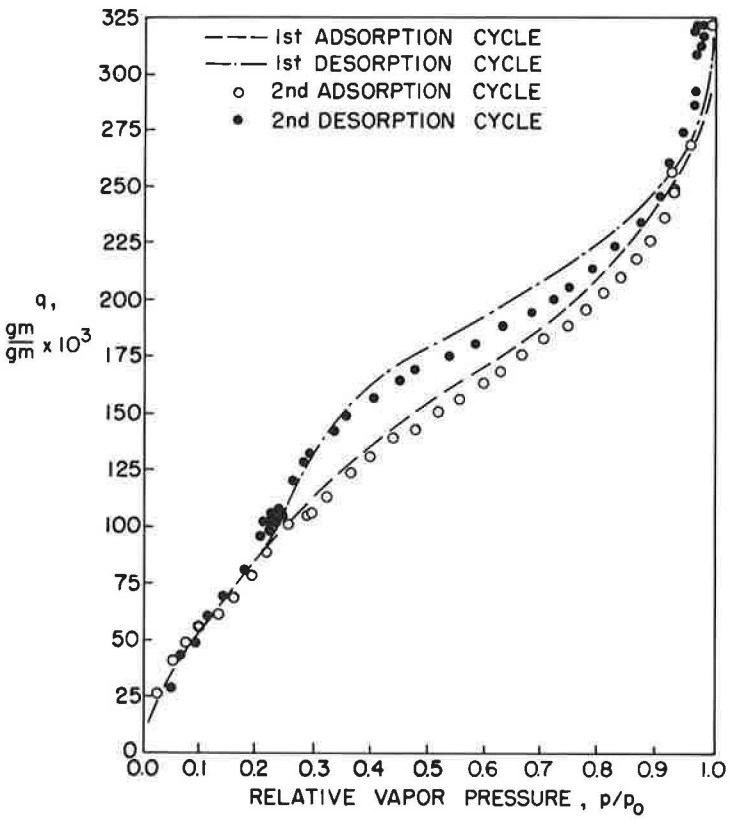

Figure 8. Sorption isotherms of calcium montmorillonite, first and second cycles.

move the water from within the collapsed clay structure. Hence, the values for the BET function, the Langmuir function, and the free energy change for the second cycle were computed from the isotherm beginning at q = 0 and using the end point of the first desorption cycle as the new reference point.

The isotherms show equilibrium moisture contents for the clay as the relative water vapor pressure increases or decreases. In the low relative pressure region the isotherm is concave to the pressure axis, whereas in the high relative pressure region it is convex to the pressure axis. In an intermediate pressure range the isotherm exhibits a somewhat linear portion, the length and slope of which Brunauer (11) states is dependent on the adsorbent, the adsorbate and the temperature selected for the investigation. Orchiston (38, 39) points out that the multimolecular adsorption theory is based on an adsorption on localized sites rather than on the formation of a mobile adsorbed layer. Using the Orchiston (39) approach, the concave section of the isotherm explains the completion of the first layer on these sites which may grow vertically and horizontally. The convex section of the isotherm shows a running together of the clusters of water molecules around the active sites.

It can be seen that there is a drift on successive cycles with the same adsorbent, and the isotherms do not coincide. The shift in the curve is probably due to a rearrangement of the surface areas as well as the changes due to pore size and shape during the first adsorption cycle. In the relative pressure range from $p/p_o = 0.85$ to saturation, the effects due to capillary condensation are pronounced.

Several interesting facets concerning the rate of adsorption were observed during the investigation. The spontaneity and instantaneousness of adsorption was indicated by the automatic recording device attached to the electrobalance. As soon as a small increment of water vapor entered the system, the response of the pen was immediate. At low relative pressures, the slope of the line described by the marking pen was very steep, and the slope decreased as the relative vapor pressure approached saturation. During desorption studies, this trend was reversed at high relative vapor pressures. If it is assumed that only a small fraction of the impinging water vapor molecules are reflected back elastically by the solid, the rate of adsorption on a free surface would be quite rapid. If, however, the adsorbent contains long, very narrow pores and the vapor must diffuse into them, the adsorption would take a longer time to reach equilibrium. If the incoming water molecules must displace any previously adsorbed molecules already there, the rate of adsorption may become very slow. In these studies, equilibrium was reached four hours after introduction of vapor and eight hours after removal of vapor for adsorption and desorption respectively. At low pressure, approximately 90 percent of adsorption took place within the first 24 minutes after the valve controlling the water reservoir was closed.

A similar trend was observed with the X-ray diffraction studies. After introducing a small amount of water vapor, the goniometer was set in motion, starting at a 2θ angle two to four degrees lower than the apparent basal spacing for the previous transfer. The shift to the new vapor transfer peak position was observed within two minutes after stopcock S-1 was closed (Fig. 1). At all relative vapor pressures up to $p/p_o = 0.98$, the new peak position determined within 30 minutes after closing the stopcock did not change in position or intensity during the next 24 hours. This would indicate that the basal spacing and intensity both change rapidly with the introduction of vapor. The shift in basal spacing was dependent on the amount of water adsorbed.

For the final expansion or initial collapse of highly hydrated calcium montmorillonite there is either a force or strain to be overcome and/or the pores must be sufficiently filled or evacuated.

Barrer and MacLeod (3) studied the sorption of non-polar and polar gases and vapors on montmorillonite. They reported that in theory Van der Waals adsorption should take place instantaneously, but that conducting of heat away from the sample causes a slight time lag. Additional slowing down is due to diffusion of vapors between particles of adsorbent, and redistribution of sorbed vapors by evaporation and condensation which proceeds until a uniform distribution of adsorbed material throughout the sample is achieved.

Brunauer (11), Foster (20), and McBain (31) have shown that hysteresis can be expected with porous adsorbents. The adsorption and desorption isotherms fall on different curves forming a hysteresis loop which closes in the range of $p/p_o = 0$ to $p/p_o = 0.25$. The hysteresis loop indicates more adsorbate during desorption than during adsorption at a given pressure. Physical adsorption on the surface of the adsorbent is usually completely reversible, whereas the hysteresis shown by the desorption branch may or may not be reversible. If on repeating the experiment the desorption isotherm is completely reproduced, the desorption hysteresis can be considered as reversible; or it is irreversible if the second investigation gives a different curve. We may note that the hysteresis begins in the region of multimolecular adsorption.

The first explanation for hysteresis was advanced by Zsigmondy in terms of capillary condensation (11, p. 394). He assumed that during adsorption the vapor does not wet the walls of the capillaries in which absorption takes place. As the adsorption reaches saturation, the impurities are displaced and at saturation complete wetting takes place. The hysteresis due to trapped gases or adsorbed water molecules should be eliminated or reduced by effective evacuation of the system prior to investigation.

Barrer and MacLeod (3) have explained hysteresis by stating that the desorption branch is the delay of the development of an adsorbate-poor phase in the interlayer regions caused by strain and interfacial free energy until the pressure of the system has fallen below that for true equilibrium, whereas for adsorption, the development of an absorbate-rich phase in the interlayer regions is delayed due to strain and interfacial tensions and the pressure exceeds the value for true equilibrium between the vapor and separated montmorillonite layers with or without interlayer adsorbate.

Hirst (25) has shown that the forces tending to hold platelets together also prevents penetration of the adsorbate. Interlayer adsorbate can only enter after a sufficient pressure is reached which would overcome the attractive forces and allow penetration. As the solid swells on adsorption, the free energy lowering of the solid may not be equated to the free surface energy since some energy will be used as work of expansion. As the interlayer attraction is reduced by the expansion, less energy is necessary to expand the unit for additional penetration of vapor. Brunauer (11) points out that even though adsorbents are usually regarded as rigid bodies, the adsorption process causes a change in pore volume, shape, and a rearrangement of the surface of the sample.

The plot in Figure 8 tends to produce a completely reproducible isotherm up to $p/p_o = 0.20$, after which a well-defined hysteresis is observed. This is consistent with the studies conducted by Bering et al (6) on bentonite using hydrocarbons as well as water vapor. Demirel (16) and Roderick (43, 44) observed that the adsorption branch of the homoionic bentonites investigated gave better reproducibility, and they chose the adsorption branch as the true equilibrium curve. Mooney et al (35, 36) observed that during their water vapor montmorillonite studies, the adsorption isotherm was not reproducible, and they apparently used the initial water content at which the adsorption was begun. The desorption isotherm had a hysteresis which was reproducible, and because of the irreversibility of hysteresis and the close reproducibility of the desorption curves, they chose the desorption curves as the true equilibrium curves.

Adsorption Models

According to Martin (32), the adsorption of water vapor on montmorillonite is a very complex process and it is very difficult to properly ascribe the phenomena to one single model of adsorption such as the Langmuir model or the multimolecular adsorption model for the entire range. It can be seen that the repeated cycles do not give a straight line for the Langmuir model, indicating that the Langmuir equation

$$\frac{\frac{p}{p_o}}{q} = \frac{1}{ab} + \frac{\frac{p}{p_o}}{b}$$

is not obeyed. The isotherm was therefore subdivided into a number of straight-line portions to determine if in the region between p/p_o equal to 0.0 to 0.28 any substantial

information could be obtained concerning unimolecular adsorption. Brunauer (11) has pointed out that a similar technique was applied to the adsorption of chlorine by silica gel, and attributed straight-line relationships for the various sections to adsorption on fractions of the surface that had roughly the same heat of adsorption. The sample under investigation had a crystalline surface, and one should expect several surface types corresponding to the different developed crystal faces.

Van Olphen (48) conducted water vapor experiments on a sodium vermiculite to give clues for the interpretation of the intercrystalline swelling of montmorillonite. He determined that the second monomolecular layer of water entered only after the first layer was completed, and his isotherms showed a definite stepwise trend. Van Olphen's Langmuir plot gave linear relations, and "one-layer" and "two-layer" Langmuir plots were defined from the data. However, plots for the present investigation indicate that for Wyoming calcium bentonite, the Langmuir treatment does not give reasonable results (Fig. 9).

The multimolecular adsorption (BET) theory was developed in 1938 by Brunauer, Emmett, and Teller (11, 12). For adsorption on a free surface utilizing relative vapor pressures, they derived the equation

$$\frac{\frac{p}{p_o}}{V\left(1 - \frac{p}{p_o}\right)} = \frac{1}{V_m C} + \frac{C - 1}{V_m C}\left(\frac{p}{p_o}\right) \qquad (3)$$

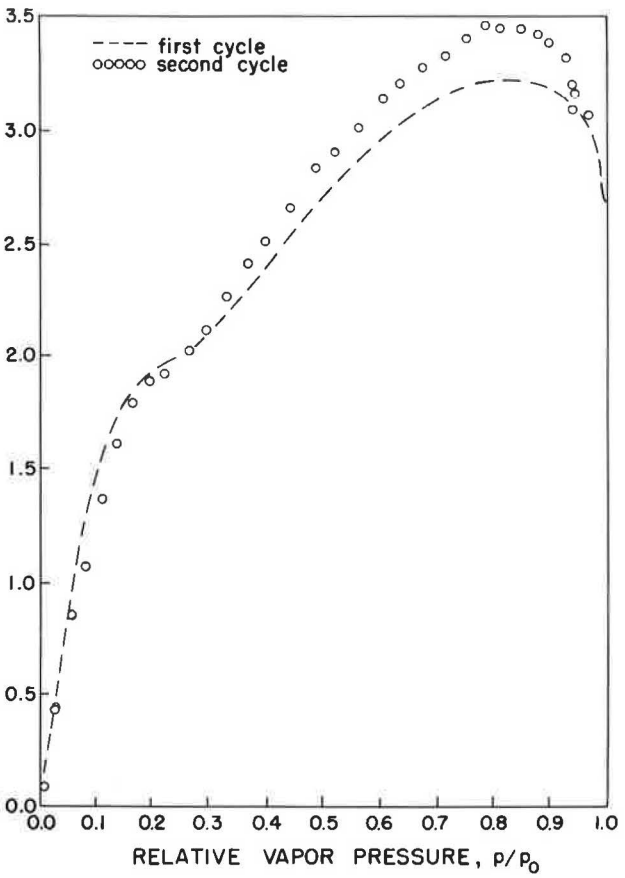

Figure 9. Langmuir plot for the adsorption of water vapor on calcium montmorillonite.

where V is the volume of vapor adsorbed at pressure p, V_m the volume of the vapor adsorbed when the surface of the adsorbant is covered by a monomolecular layer of adsorbate, and p_o is the saturation pressure. The constant C can be determined by the equation

$$C = e^{(E_1 - E_L)/RT} \tag{4}$$

where E_1 is the average heat of adsorption in the first layer and E_L is the heat of liquification.

Equation 3 becomes

$$\frac{\frac{p}{p_o}}{q\left(1 - \frac{p}{p_o}\right)} = \frac{1}{q_m C} + \frac{C - 1}{q_m C}\left(\frac{p}{p_o}\right) \tag{5}$$

when the amount of vapor adsorbed is determined in terms of mass where q is the mass of the vapor adsorbed at pressure p and q_m is the mass adsorbed at monolayer coverage at the adsorbant surface.

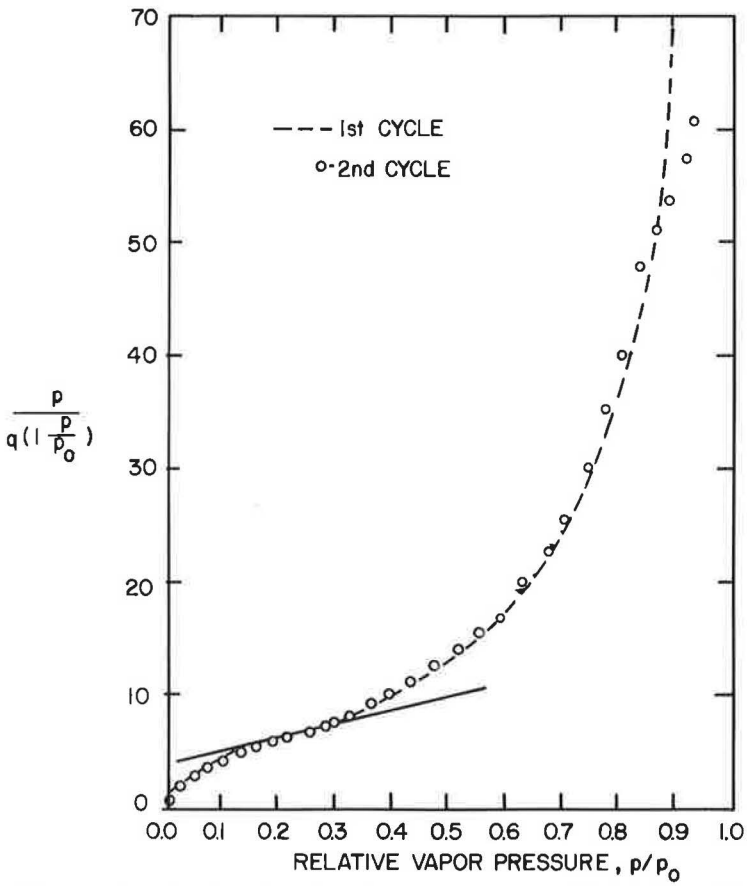

Figure 10. BET plots for the adsorption of water vapor on calcium montmorillonite.

The BET multimolecular adsorption model gives a reasonably straight line in the region of p/p_o from 0.11 to 0.27. The region normally expected for the multimolecular adsorption model to be obeyed is between $p/p_o = 0.05$ and $p/p_o = 0.35$.

The BET plot in Figure 10 gives reasonably good straight lines within the range of applications from 0.11 to 0.27 relative pressures. The parameters q_m and C were calculated by a least-squares treatment of all the experimental data for both cycles. In order to estimate the accuracy of the values in the equation, the method proposed by Topping (46, p. 105) was used. The equation of the line obtained is

$$y = (6.523 \pm 0.0625)x + (1.682 \pm 0.0120)$$

When the slope of the line and the intercept are known, the equation enables one to determine q_m and C. The values of these parameters are 0.1219 gm/gm and 4.878, respectively. The errors in q_m and C were calculated from the principle of superposition of errors.

The values of q_m and C corrected for the errors noted above are 0.1219 ± 0.0009 gm and 4.878 ± 0.042, respectively. The data show very little error from a straight line determined by the least-squares method for the BET data; departures from the straight line after p/p_o of 0.27 are probably somewhat complicated by capillary condensation, although of a minimal nature at this low range of p/p_o.

The X-ray data indicate that initial separation of the platelets starts almost immediately as the relative pressure increases from zero. However, from p/p_o of 0.00 to 0.02 there is very little increase in spacing, indicating perhaps initial adsorption on the external surfaces. After 0.02, the spacing starts to increase rapidly with an increase in pressure, indicating that the preponderance of water adsorbed is interlayer water.

The problem of external area coverage as applied to the montmorillonite system might better be termed the areas accessible to polar and non-polar gases and vapors. As pointed out previously, nitrogen is adsorbed only on external surfaces. If a single non-swelling platelet is considered, then the area available to nitrogen and water vapor would be the same as indicated in Figure 11a. On the other hand, if the system is constituted of a porous swelling powder, as is the system under investigation, then the area available to water might be considerably greater than that available to nitrogen, as in Figure 11b. The smaller water molecules perhaps can either be accommodated in narrower intercrystalline channels or can penetrate into tapered channels that are inaccessible to nitrogen molecules. By using the Kelvin equation, one can see that as the relative pressure increases, the capillary radius available to a molecule for capil-

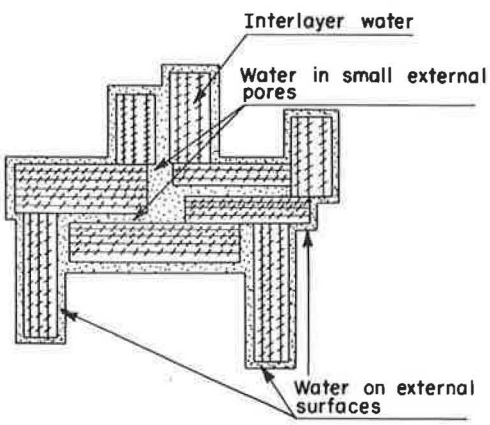

Figure 11a. Idealized diagram of possible areas accessible to water.

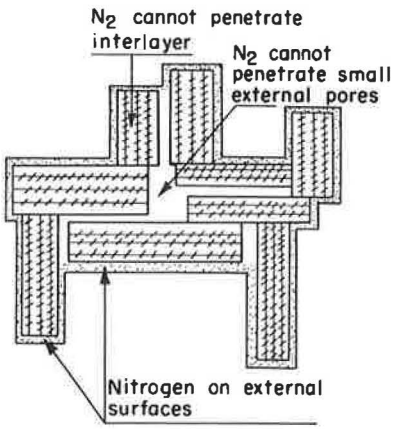

Figure 11b. Idealized diagram of possible areas accessible to nitrogen.

lary condensation increases. Therefore, the following situation may occur with respect to montmorillonite powders.

In Figures 11a and 11b, the pore spaces between the platelets act as capillaries and are accessible to water molecules when the diameter of the pore spaces is such as to allow the passage of a water molecule with diameter of 2.76 Å. The water will penetrate between platelets as well as external areas, and the area available to water would be the total external area as well as the internal area of the agglomerate of platelets. In the case of nitrogen adsorption, when the pore spaces are too small in diameter to pass the 4.5 Å nominal diameter nitrogen molecule, the areas within the platelets' agglomerate would not be accessible to the molecule. Therefore, the area associated with the nitrogen would be the external area of the agglomerate only. Roderick (43) found that the sodium montmorillonite area determined by water adsorption varied from 83 to 145 m^2/gm to 172 m^2/gm. Both values of Roderick are considerably larger than those reported by others as determined from nitrogen adsorption, i.e., 41 to 71 m^2/gm by Emmett (29), 33 m^2/gm by Mooney et al (36), and 34.5 m^2/gm by Zettlemeyer et al (50).

Heat of Adsorption

Brunauer (11) points out that the criteria of the application of the BET theory was based on the reasonableness of the two parameters q_m and C evaluated from the straight lines. The average heat of adsorption less the heat of liquification of the first observed monomolecular layer was calculated by using Eq. 4 to obtain

$$E_1 - E_L = R\,T \ln C = 1.987 \times 298.16 \times \ln C \text{ cal/mole}$$

However, this value for the heat of adsorption required a correction when C was rederived by Clampitt and German (15). By using their correction, the equation for calculation of E_1 becomes:

$$E_1 - E_L = R\,T \ln C + (\Delta H_s - E_L) \qquad (5)$$

where ΔH_s is the heat of vaporization of the surface layer, and $(\Delta H_s - E_L)$ accounts for the difference in the heat of vaporization of successive layers and is equal to -1.7 kcal/mole (15). Both corrected and uncorrected values are listed in Table 3 for several calcium montmorillonites for which water vapor adsorption data are available, and show reasonably good uniformity.

Free Energy Changes

It is possible to determine the free energy changes that occur during adsorption of vapors on solid surfaces using the Gibbs equation. This indirect method was first

TABLE 3

AVERAGE HEAT OF ADSORPTION OF MONOMOLECULAR WATER ADSORBED ON CALCIUM MONTMORILLONITE, CALCULATED FROM BET PARAMETERS LISTED

Mineral	BET parameters		Average Heat of Adsorption Less Heat of Liquification E_1-E_L, Kcal/mole	
	q_m	C	According to Brunauer (11)	Corrected According to Clampitt and German (15)
Hendricks et al (24)[a]				
Mississippi Ca-montmorillonite	0.130	23	1.9	3.6
California Ca-montmorillonite	0.133	15	1.6	3.3
Wyoming Ca-montmorillonite	0.125	6	1.1	2.9
Demirel (16)				
Wyoming Ca-montmorillonite	0.130	6.7	1.1	2.8
Wyoming Ca-montmorillonite[b]	0.1219	4.878	0.94	2.6

[a] BET parameters calculated by Demirel (16, Figs. 24 and 25).
[b] BET parameters calculated by data in this study.

proposed by Bangham and Razouk in 1937 (1, 2). Their treatment was vigorously applied to nonporous solids (7, 27) and later the method was shown to apply for porous adsorbent and not to depend on the degree of compression (5, 17, 21).

Boyd and Livingston (7) have shown that if the adsorption isotherm for a vapor on a crystalline nonporous powder is obtained and if the specific surface area is determined by the BET method (11), the change in free energy of a clean solid surface upon immersion in a saturated vapor can be calculated. Using the Gibbsian adsorption, Boyd and Livingston derived an equation for the free energy of immersion of a nonporous wettable surface in a saturated vapor. When relative vapor pressures are employed, it can be made to read

$$\Delta F = (\gamma_{s\ell} - \gamma_{so} + \gamma_{\ell v}) = -\frac{RT}{M\Sigma}\int_0^1 \frac{q}{\frac{p}{p_o}}\, d\left(\frac{p}{p_o}\right) \tag{6}$$

where $\gamma_{s\ell}$ is the solid liquid interfacial tension, γ_{so} the surface tension of the solid in a vacuum, $\gamma_{\ell v}$ the surface tension of the liquid in contact with its own vapor, q is the mass of vapor adsorbed by a unit mass of the solid, and p/p_o is the relative vapor pressure.

The clay mineral investigated consists of a solid powder absorbent that has a rigid structure. This structure is not influenced by the adsorption of water vapor except as far as the adsorbate enters the interstices of the interacting solid surface and causes swelling between the platelets. This separation is manifested in separation against the forces of interaction (27), and the equation for the free surface energy must be modified as given by Demirel (16):

$$\Delta F = (\gamma_{s\ell} - \gamma_{so}) + \alpha \Delta V \tag{7}$$

where ΔF is the free energy change of wetting of the solid by the liquid, ΔV is the change in potential energy of interaction, or the free energy per square centimeter of the intersticial surface due to the separation of particles against the force of interaction, and α is the interfacial surface area per square centimeter of total surface (40, p. 253).

The values of the function $q/(p/p_o)$ versus p/p_o used to determine the free energy changes are plotted in Figure 12 for the first and second adsorption cycles, respectively. Demirel (16) and Roderick (43, 44) used similar plots to determine the free energy of wetting in their studies of montmorillonites.

The second adsorption cycle agrees with the first cycle up to approximately p/p_o = 0.3. From p/p_o = 0.3 to 0.9, the first cycle points were from 0 to 12 mg/gm higher than the second cycle. Between p/p_o = 0.9 and saturation, the second cycle points passed through the curve of the first cycle. Slight changes in the pore size and shapes would cause this difference. However, since the second adsorption points agree with the first cycle in the low-pressure region and very nearly agree up to p/p_o = 0.40, any slight swelling of the pores or material after the first cycle would not materially change the calculated free energy of wetting because the low pressure data are of the most importance in the energy change calculations.

The free energies of wetting were actually calculated by using Eq. 6 and a graphical integration of the curves presented in Figure 12.

The errors in the function were estimated to be ±0.013 and ±0.015 for the first and second adsorption cycles, respectively. The numerical values for the integral $\int \frac{q}{p/p_o}\, d\left(\frac{p}{p_o}\right)$ were found to be 0.3858 and 0.3844 ± 0.015 gm/gm of calcium montmorillonite for the first and second adsorption cycles, respectively. The specific surface Σ for Eq. 6 was determined from crystallographic data (47) for calcium montmorillonite by the relationship

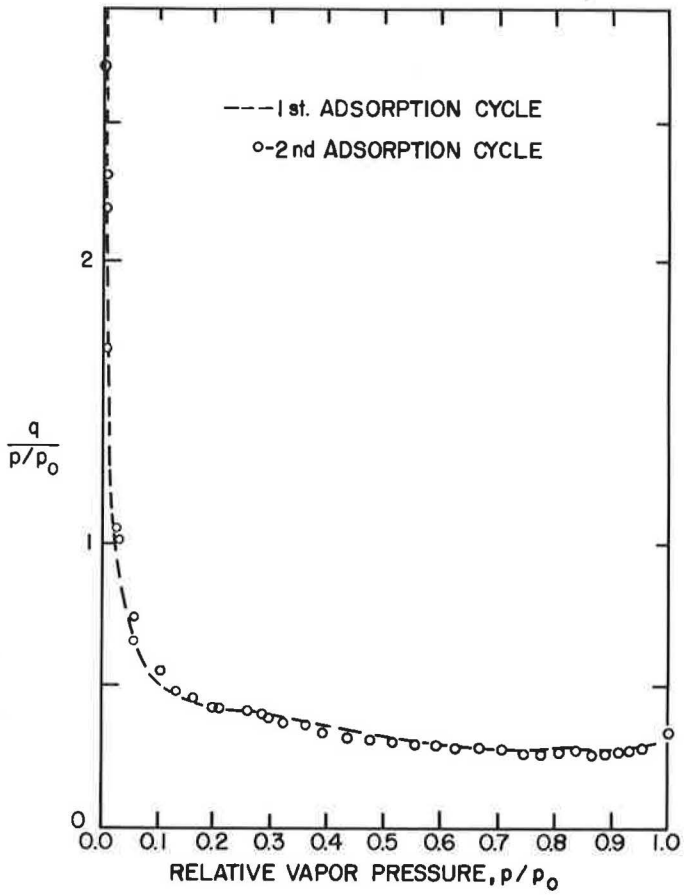

Figure 12. Plot for the graphical integration of the equation for the adsorption of water vapor on calcium montmorillonite.

$$\Sigma = \frac{N_A}{M_{ca}} \sigma \tag{8}$$

where N_A is Avogadro's constant, M_{ca} is the weight of the calcium montmorillonite unit cell, and σ is the area exposed by one unit cell layer. M_{ca} is equal to 732. The value of σ may be determined from the unit cell dimensions $a_o = 5.16$ Å and $b_o = 8.94$ Å. Substituting these values in the expression above, the specific area is found to be

$$\Sigma = \frac{6.02 \times 10^{23} \times 2 \times 5.16 \times 8.94}{732 \times 10^{10} \times 10^{10}}$$

$$\Sigma = 759 \text{ m}^2/\text{gm}$$

Using the value of the parameter q_m obtained in the BET solution, the specific surface was also calculated:

$$\Sigma = \frac{N_A \, q_m \, s}{M} \tag{9}$$

Substituting the values of $q_m = 0.1219$ and $s = 17.5$ Å^2 per molecule of water vapor in Eq. 9, the specific surface was found to be

$$\Sigma = \frac{6.02 \times 10^{23} \times 0.1219 \times 17.5}{18.02 \times 10^{10} \times 10^{10}}$$

$$\Sigma = 714 \text{ m}^2/\text{gm}$$

The value obtained by using the BET parameter is a reasonable value and compares very well with the theoretical crystallographic data. When Σ obtained from Eq. 8 is substituted in the equation, the free energy of immersion in saturated vapor or liquid, also referred to as the free energy of wetting, is calculated as follows:

$$\Delta F = -\frac{RT}{M} 0.3858$$

$$= -\frac{8.314 \times 10^7 \times 298.16}{18.02 \times 759 \times 10^4} \times 0.3858$$

$$\Delta F = -69.91 \pm 2.36 \text{ ergs/cm}^2$$

$$\Delta F = -\frac{8.314 \times 10^7 \times 298.16}{18.02 \times 759 \times 10^4} \times 0.3844$$

$$\Delta F = -69.66 \pm 2.72 \text{ ergs/cm}^2$$

Demirel (16) reported a value of -76.61 ± 4.30 ergs/cm^2 for calcium montmorillonite. He used a loose powder in his study, yet the values obtained in both studies are in very good agreement. Craig et al (14) found similar results in their studies of compressed and uncompressed graphite powders, pointing out the importance of accurate low pressure range data.

Expansion Energies

Fu and Bartell (21), studying the surface areas of porous absorbents, evaluated Eq. 6 and found that the change in free energy could be expressed by the relationship

$$\Sigma \Delta F = \alpha (p/p_o)^{\beta}$$

where ΔF is the decrease in the free energy per unit area, α and β are constants, p/p_o is the relative vapor pressure, and Σ is the area on which the adsorption takes place. They point out that this method can be utilized to study the expansion and deformation of porous materials caused by adsorption of various vapors. For a given adsorbate-adsorbent system, α and β remain constant so long as there is no change in the mechanism of adsorption. If changes in the mechanism of adsorption, such as capillary condensation or swelling occur, values of α and β change to another set of constant values. If only the external surface areas of the clay are involved in adsorption of the vapor, the relationship can be made to read:

$$\Sigma_{ext} \Delta F = \alpha (p/p_o)^{\beta}$$

The change in slope of the $\Sigma\Delta F$ curve observed by Fu and Bartell (21) was attributed to capillary condensation in the pores of the adsorbents. The exact point at which capillary condensation takes place cannot be determined, but it may be assumed to show its most pronounced effects at p/p_o values greater than 0.9 to saturation. For clay min-

erals, while capillary condensation undoubtedly has some effect, swelling (interlayer expansion) manifests itself more profoundly throughout the entire adsorption range.

The values of the integral

$$-\frac{RT}{M}\int_{0}^{p/p_o=1}\frac{q}{\frac{p}{p_o}}\,d\left(\frac{p}{p_o}\right) = \Sigma\Delta F$$

for increasing values of p/p_o from zero to saturation for the adsorption were plotted on log-log paper with $\Sigma\Delta F$ on the vertical axis and p/p_o on the horizontal axis (Fig. 13). A close examination of the plot indicates six straight-line portions, the breaks occurring at $p/p_o \doteq 0.01$, $p/p_o = 0.065$, $p/p_o = 0.19$, $p/p_o = 0.85$, and $p/p_o = 0.98$. From the X-ray data, the initial adsorption at low relative pressures from zero to approximately 0.01 occurs on the external surface areas. Therefore, the straight-line portion of the log-log plot corresponding to a p/p_o range of 0 to 0.01 (not shown in Fig. 13) was extrapolated to saturation, as indicated by a dashed line, assuming that the free energy relationship of Fu and Bartell (21) was obeyed. The differences between the extrapolated curve and the plot $\Sigma\Delta F$ is the free energy change of internal surfaces (expansion energy). This relationship may be expressed as

$$\Sigma_{int}\,\Delta F_i = \Sigma\Delta F - \Sigma_{ext}\,\Delta F_e$$

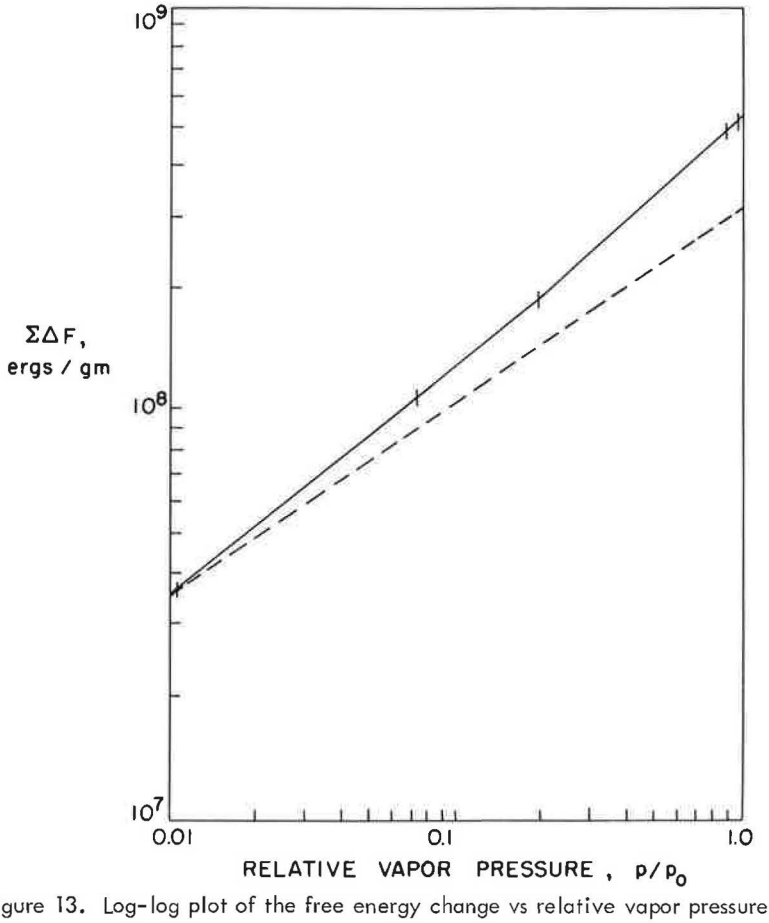

Figure 13. Log-log plot of the free energy change vs relative vapor pressure.

where Σ_{ext} is the external surface area, Σ_{int} is the internal surface area, Σ is the specific surface area, and ΔF_i is the expansion energy per square centimeter of internal surface; ΔF_i may be expressed in terms of an equation as follows:

$$\Delta F_i = (\gamma_{s\ell} - \gamma_{so}) + \Delta V$$

where ΔV is the free energy change per square centimeter of internal surface due to the separation of the particles against the force of interaction. ΔF_i can be calculated by the expression

$$\Delta F_i = \frac{\Sigma \Delta F - \Sigma_{ext} \Delta F_e}{\Sigma_{int}} \qquad (10)$$

and $\Sigma_{int} \Delta F_i$ may be obtained from Figure 13 as the difference between the plot of $\Sigma \Delta F$ and the dashed line extended to saturation, indicating the change in free energy due to adsorption on external surfaces.

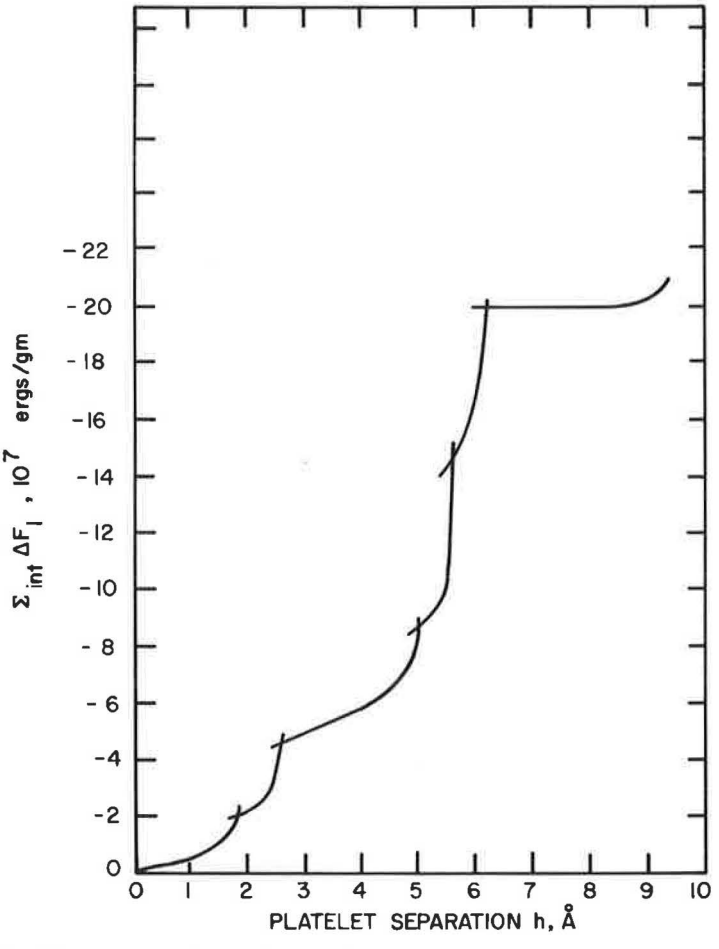

Figure 14. Plot of free energy change due to adsorption on and separation of internal surfaces vs interlayer separation.

Figure 14 is a plot of $\Sigma_{int} \Delta F_i$ vs platelet separation h. It can be seen that the changes in slope of the free energy change with increasing relative vapor pressure. Figure 14 can be conveniently divided into four major segments: segment I from 0 to 2.6 Å, segment II from 2.6 Å to 5.1 Å, segment III from 5.1 Å to 6.2 Å, and segment IV from 6.2 Å to 9.1 Å. The free energy change in segments I and II is about equal. The free energy change for segment III is substantially greater than a combination of the three other segments.

The expansion energy of the first segment is the free energy change which includes the disappearance of the solid surface forming a solid-adsorbed film interface, and the partial hydration of the adsorbed cation plus the contribution due to separation against the force of interaction between platelets. This latter term will decrease the magnitude of the free energy change. As the adsorption continues (segment II), the second layer of water penetrates between the first layer and the surface, and the free energy change is due to the extension of the film thickness and is probably less than that for disappearance of the solid surfaces and formation of a solid-adsorbed film interface. However, since the distance between the platelets is greater than that corresponding to the previous step, the interaction between platelets is decreased. In segment III, additional vapor is adsorbed in the interlayer region, further slightly reducing the interaction forces. In this segment, the free energy change is quite large because of the arrangement of the water molecules covering the active sites. No new surfaces appear or disappear. The free energy on adsorption for the final expansion, segment IV, is due to penetration of additional water molecules between the layers. The forces of interaction between the platelets are relatively far removed from each other.

Since the free energy change for segment IV is the smallest of any of the segments, the energy for penetration of water molecules between the water complexes existing must be less than for penetration between the clay surfaces, or due to hydration of the cations and arrangement of water molecules in the interlayer regions.

Swelling Pressures

The change in free energy at constant temperature can be expressed as

$$dF = V\, dp \tag{11}$$

where V is the molar volume of the adsorbed water and p is the external pressure. However, if we consider that the expansion is due only to the adsorption of vapor on the interlayer surfaces, the expression may be made to read

$$\Sigma_{int}\, dF_i = V\, dp \tag{12}$$

Since water is incompressible this equation becomes

$$dF_i = \frac{V}{\Sigma_{int}}\, dp = h_o\, dp \tag{13}$$

where dF_i is the expansion energy per square centimeter, V is the total volume of the interlayer at saturation per gram of calcium montmorillonite, h_o is the maximum platelet separation, and p is the applied pressure. When Eq. 13 is integrated, we obtain the following:

$$\Sigma_{int} \int_{\Delta F_s}^{\Delta F_i} dF_i = \Sigma_{int} \int_{p=0}^{p} h_o\, dp$$

$$p = \frac{\Sigma_{int}\, \Delta F_i - \Sigma_{int}\, \Delta F_s}{h_o\, \Sigma_{int}} \tag{14}$$

where ΔF_s is the expansion energy when clay is in equilibrium with saturated vapor, p is the pressure required to prevent any platelet separation, and p = 0 is the pressure when the maximum separation is obtained. From Figure 14 the expression Σ_{int} ΔF_i - Σ_{int} ΔF_s for the expansion energy may be obtained for platelet separation h and h_o, respectively. The swelling pressure may now be found by dividing the expression by the maximum platelet separation and the calculated internal surface area. Table 4 is a computation of expansion energies and swelling pressures for the calcium montmorillonite under investigation.

The internal area used in the table was calculated using three different values for the cross-sectional area of adsorbed water molecules and the value of q_m for the external area obtained from the BET equation. Hendricks and Jefferson (23) reported a laminar stacking of interlayer water such that the area occupied by a water molecule is 11.5 Å^2. The area occupied per molecule of closest packing would be 10.8 Å^2. The data in the present study suggest an ice-like configuration of water similar to the one proposed earlier (16) which gave a cross-sectional area of 17.5 Å^2. Use of these three values in Eq. 9 gave the calculated external surface areas. Internal areas were determined by subtracting each external area from the total surface of 759 m^2/gm obtained from crystallographic data. The values for the internal areas were 653 m^2/gm for 10.8 Å^2, 646 m^2/gm for 11.5 Å^2, and 587 m^2/gm for 17.5 Å^2.

Van Olphen (47) used the desorption data of Mooney et al (35, 36) to estimate the pressure required to remove one monolayer of water from clay surfaces, by dividing the free energy change by the thickness of one monolayer of water. He found the energy required to remove the interlayer water from between clay platelets to be from 50 to 100 ergs/cm^2 or 630 to 1260 tons/ft^2.

Roderick (43, 44) obtained a total free energy change of 40.55 ergs/cm^2 using a sodium Wyoming bentonite, and using the method outlined above he obtained swelling pressure values from 52 tons/ft^2 to 339 tons/ft^2. The sodium montmorillonite did not swell initially and he was able to determine accurately an external area. Determining the external area in this study was more difficult since only a very short range of relative pressure was observed where the adsorption was chiefly on the external surfaces.

TABLE 4

EXPANSION ENERGIES AND SWELLING PRESSURES FOR INDICATED SEPARATIONS DUE TO ADSORPTION OF WATER VAPOR ON THE INTERLAYER SURFACES OF CALCIUM MONTMORILLONITE

Separation	Area Assigned to a Water Molecule, Å	Internal Surface Area, m^2/gm	Expansion Energy ergs/cm^2	Swelling Pressure, p, dynes/cm^2	Swelling Pressure, tons/ft^2
No interlayer water present	10.8	653	–	377	394
	11.5	646	–	382	399
	17.5	587	–	419	437
One molecular layer of interlayer water	10.8	653	3.1	370	386
	11.5	646	3.1	374	390
	17.5	587	3.4	412	430
One molecular layer of interlayer water plus start of cation hydration	10.8	653	6.9	268	280
	11.5	646	7.0	271	283
	17.5	587	7.7	298	311
Two molecules of interlayer water (laminar stacking)	10.8	653	14.7	176	184
	11.5	646	14.9	180	188
	17.5	587	16.4	198	210
Three molecular layers of interlayer water	10.8	653	22.2	83	87
	11.5	646	22.4	85	89
	17.5	587	24.7	93	97
Four molecular layers of waterlayer water in tetrahedral coordination (ice-like configuration)	10.8	653	30.6	37	38
	11.5	646	31.0	37	38
	17.5	587	34.1	41	43
Five layers of interlayer water	10.8	653	31.2	—	—
	11.5	646	31.6	—	—
	17.5	587	34.7	—	—

The data at relative vapor pressures between zero and $p/p_o = 0.01$ are limited and the extrapolation of the straight line indicating the free energy change due to adsorption on external surfaces in Figure 14 may not be as accurate as those determined by Roderick (43, 44).

By using the procedures outlined, the uplift pressures for calcium montmorillonite were found to vary from 38 tons/ft^2 to 437 tons/ft^2, higher at lower relative pressures.

CONCLUSIONS

1. Upon adsorption or desorption of water, the first-order basal spacing of calcium montmorillonite varies in a continuous but nonuniform manner.

2. X-ray diffraction line breadths are a minimum for basal spacings of 16.5 and 19.2 Å, suggesting uniform layer separations at these spacings. Simultaneously the diffraction intensity decreases, indicating that the interlayer water has structure. Combining X-ray with adsorption data indicates that at 16.5 Å the water has an ice-like configuration; the 19.2 Å spacing and sorption data may be explained by intrusion of one additional layer of water.

3. At vapor pressures which give basal spacings less than 16.5 Å, line breadth and intensity data suggest simultaneous existence of varying numbers of water layers between the platelets, and steps in the basal spacings appear to be directly influenced by the interlayer cations.

4. At certain vapor pressures and d_{001} spacings, strong secondary basal reflections appeared in the neighborhood of 3 Å and 5 Å, and may be explained by use of an electron density curve inferred from the mica-like structure of the clay layers.

5. Interlayer swelling and shrinkage of calcium montmorillonite due to adsorption of water exhibit a hysteresis forming two loops, one from relative vapor pressure of zero to about 0.40 and the other from about 0.55 to saturation. X-ray diffraction line breadths during desorption suggest that at low pressures the water is very strongly attracted to the surfaces or around cation positions forming islands of water within the interlayer regions. As the sheets become undulated, the water may be trapped and the escape of water to the vapor environment is inhibited. The hysteresis in the high relative vapor pressure region is accompanied by an increase and then decrease of line breadth as the fourth and fifth layers of water are withdrawn. This water escapes quite easily indicating that it is not as strongly oriented as the water near the surface of the platelets.

6. Calcium montmorillonite shows coloration after X-radiation. This was attributed to prolonged X-radiation induced color centers.

7. The sorption isotherms are completely reversible at a relative vapor pressure between zero and 0.20. The adsorption isotherms are more closely reproducible on successive cycles and the rate of adsorption is greater than desorption as observed from the automatic recording device and X-ray diffraction pattern, suggesting that the adsorption branch is the equilibrium branch.

8. The BET multimolecular adsorption model more closely fits the experimental data than does the Langmuir monomolecular adsorption model.

9. The experimentally determined total surface area calculated from the BET parameter q_m is equal to 714 m^2/gm, which is in good agreement with the 759 m^2/gm calculated from crystallographic data.

10. The BET parameter C was used to determine the heat of adsorption of the first molecular layer of water on calcium montmorillonite less the heat of condensation of water ($E_1 - E_L$) and was found to be 2.6 kcal/mole, which agrees favorably with previously published data.

11. The free energy of wetting, defined as the free energy of immersion less the free energy change due to particle interaction, was found on a compressed calcium montmorillonite powder to be -69.91 ± 2.30 ergs/cm^2 and -69.61 ± 2.72 ergs/cm^2 for the first and second adsorption cycles, respectively. This is in good agreement with data of Demirel (16), who obtained -76.61 ± 4.30 ergs/cm^2 using a loose powder. The magnitude of the free energy change is not affected by the degree of compression of the powder. The low-pressure region data are most important for determining free energy changes.

12. The X-ray diffraction data and adsorption isotherm data were used to estimate the external surface area at low relative vapor pressure regions. The free energy was divided into two components, one due to absorption on interlayer surfaces and particle interaction and the second to adsorption on external surfaces. These data enable one to estimate the expansion energies and uplift pressures. The swelling pressures exerted with the platelet separation corresponding to zero to four layers of water are 440 tons/ft^2 to 40 tons/ft^2, respectively.

ACKNOWLEDGMENT

This research was done at the Engineering Research Institute, Iowa State University, under Project 665-S, "X-Ray Diffraction Analysis of Highway Materials." The project was sponsored by the Iowa Highway Research Board under Project H.R. 128 and was supported with funds from the Iowa State Highway Commission.

REFERENCES

1. Bangham, D. H. The Gibbs Adsorption Equation and Adsorption on Solids. Trans. Faraday Soc., Vol. 33, pp. 805-811, 1937.
2. Bangham, D. H., and Razouk, R. I. Adsorption and Wettability of Solid Surfaces. Trans. Faraday Soc., Vol. 33, pp. 1459-1463, 1937.
3. Barrer, R. N., and MacLeod, D. M. Intercalation and Sorption by Montmorillonite. Trans. Faraday Soc., Vol. 50, pp. 980-989, 1954.
4. Barshad, I. The Nature of Lattice Expansion and Its Relation to Hydration in Montmorillonite and Vermiculite. Am. Mineralogist, Vol. 34, pp. 675-684, 1949.
5. Bartell, F. E., and Bower, J. E. Adsorption of Vapors by Silica Gels of Different Structures. Jour. Colloid Sci., Vol. 7, pp. 80-93, 1952.
6. Bering, B. P., Dreving, V. P., Kiselev, A. V., Serpinsky, V. V., Surova, M. D., and Shoherbakova, K. D. Adsorption Properties of Montmorillonite Clays. Colloid Jour. (USSR), Vol. 14, pp. 433-441, 1952.
7. Boyd, G. E., and Livingston, H. K. Adsorption and Energy Changes of Crystalline Solid Surfaces. Jour. Am. Chem. Soc., Vol. 64, pp. 2383-2388, 1942.
8. Brindley, G. W. Chlorite Minerals. In Brown, G., editor. The X-Ray Identification and Crystal Structures of Clay Minerals. Mineralogical Society, London, pp. 242-296, 1961.
9. Brindley, G. W. Kaolin, Serpentine, and Kindred Minerals. In Brown, G., editor. The X-Ray Identification and Crystal Structures of Clay Minerals. Mineralogical Society, London, pp. 51-131, 1961.
10. Brindley, G. W. X-Ray Diffraction by Layer Lattices With Random Layer Displacements. In Brown, G., editor. The X-Ray Identification and Crystal Structures of Clay Minerals. Mineralogical Society, London, pp. 446-466, 1961.
11. Brunauer, S. The Adsorption of Gases and Vapors. Physical Adsorption. Princeton Univ. Press, 1943.
12. Brunauer, S., Emmett, P. H., and Teller, E. Adsorption of Gases in Multimolecular Layers. Jour. Am. Chem. Soc., Vol. 60, pp. 309-319, 1938.
13. Buerger, M. J. Crystal Structure Analysis. John Wiley and Sons, New York, 1960.
14. Craig, R. C., Van Voohis, J. J., and Bartell, F. E. Free Energy of Immersion of Compressed Powders With Different Liquids. I. Graphite Powders. Jour. Phys. Chem., Vol. 6, pp. 1225-1230, 1956.
15. Clampitt, B. H., and German, D. E. Heat of Vaporization of Molecules at Liquid-Vapor Interfaces. Jour. Phys. Chem., Vol. 62, pp. 438-440, 1958.
16. Demirel, T. Adsorption of Water Vapor by Sodium and Calcium Montmorillonite. Unpublished PhD thesis, Library, Iowa State University of Science and Technology, Ames, 1962.
17. Dobay, D. C., Fu, Y., and Bartell, F. E. Energetics of the Adsorption of Aliphatic Amines by Silica Gel. Jour. Am. Chem. Soc., Vol. 73, pp. 308-314, 1951.

18. Emmett, P. R., Brunauer, S., and Love, K. S. The Measurement of Surface Area of Solids and Soil Colloids by the Use of Low Temperature Van der Waals Adsorption Isotherms. Soil Sci., Vol. 45, pp. 57-65, 1938.
19. Forslind, E. Crystal Structure and Water Adsorption of Clay Minerals. Swedish Cement and Concrete Inst. Bull., Vol. 11, pp. 1-20, 1948.
20. Foster, A. G. The Sorption of Condensible Vapors by Porous Solids. I. The Applicability of the Capillary Theory. Trans. Faraday Soc., Vol. 28, pp. 645-657, 1932.
21. Fu, Y., and Bartell, F. E. Surface Area of Porous Absorbents. Jour. Phys. Colloid Chem., Vol. 55, pp. 662-675, 1951.
22. Gillery, F. H. Adsorption-Desorption Characteristics of Synthetic Montmorillonite in Humid Atmospheres. Am. Mineralogist, Vol. 44, pp. 806-818, 1959.
23. Hendricks, S. B., and Jefferson, M. E. Structure of Kaolin and Talc-Pyrophyllite Hydrates and Their Bearing on Water Sorption of Clays. Am. Mineralogist, Vol. 23, pp. 863-875, 1938.
24. Hendricks, S. B., Nelson, R. A., and Alexander, L. T. Hydration Mechanism of the Clay Mineral Montmorillonite Saturated With Various Cations. Jour. Am. Chem. Soc., Vol. 62, pp. 1457-1464, 1940.
25. Hirst, W. The Mechanical Interaction Between Mobile Insoluble Adsorbed Films, Capillary Condensed Liquid and Fine-Structured Solids. Discussions Faraday Soc., Vol. 3, pp. 22-28, 1948.
26. International Union of Crystallography. International Tables for X-Ray Crystallography. Vol. II. The Kynooh Press, Birmingham, England, 1959.
27. Jura, G., and Harkins, W. E. Determination of the Decrease of Free Surface Energy of a Solid by an Adsorbed Film. Jour. Am. Chem. Soc., Vol. 66, pp. 1356-1362, 1944.
28. Klug, H. P., and Alexander, L. E. X-Ray Diffraction Procedures for Polycrystalline and Amorphous Materials. John Wiley and Sons, New York, 1954.
29. Macey, H. H. Clay-Water Relationship and the Internal Mechanism of Drying. Trans. Brit. Ceram. Soc., Vol. 41, pp. 73-121, 1942.
30. Mackenzie, R. C. Hydrationseigenschaften von Montmorillonit. Berichte Deutsche Keram. Ges., Vol. 41, pp. 73-121.
31. McBain, J. W. An Explanation of Hysteresis on the Hydration and Dehydration of Gels. Jour. Am. Chem. Soc., Vol. 57, pp. 699-700, 1935.
32. Martin, T. R. Adsorbed Water on Clay: A Review. Nat. Conf. on Clays and Clay Minerals Proc., Vol. 9, pp. 28-70, 1960.
33. Means, R. E., and Parcher, J. V. Physical Properties of Soils. Charles E. Merrill Books, Columbus, Ohio, 1963.
34. Mering, J. On the Hydration of Montmorillonite. Trans. Faraday Soc., Vol. 42B, pp. 205-219, 1946.
35. Mooney, R. W., Keenan, A. G., and Wood, L. A. Adsorption of Water Vapor by Montmorillonite. I. Heat of Desorption and Application of BET Theory. Jour. Am. Chem. Soc., Vol. 74, pp. 1367-1371, 1952.
36. Mooney, R. W., Keenan, A. G., and Wood, L. A. Adsorption of Water Vapor by Montmorillonite. II. Effect of Exchangeable Ions and Lattice Swelling as Measured by X-Ray Diffraction. Jour. Am. Chem. Soc., Vol. 74, pp. 1371-1374, 1952.
37. Nagelschmidt, G. On the Lattice Shrinkage and Structure of Montmorillonite. Zeit. Kristallographie, Vol. 93, pp. 481-487, 1936.
38. Orchiston, H. D. Adsorption of Water Vapor. II. Clays at 25° C. Soil Sci., Vol. 78, pp. 463-479, 1954.
39. Orchiston, H. D. Adsorption of Water Vapor. III. Homoinic Montmorillonites at 25° C. Soil Sci., Vol. 79, pp. 71-78, 1955.
40. Overbeek, J. T. G. The Interaction Between Colloidal Particles. In Kruyt, H. R. Colloid Science. Vol. 1, pp. 245-277. Elsevier Publishing Co., New York, 1952.
41. Pauling, L. The Structure of the Micas and Related Minerals. Proc. Nat. Acad. Sci. U.S., Vol. 16, pp. 123-129, 1930.

42. Road Research Laboratory, Department of Scientific and Industrial Research (Great Britain). Soil Mechanics for Road Engineers. H. M. Stationery Office, London, 1954.
43. Roderick, G. L. Water-Vapor Sodium Montmorillonite Interaction. Unpublished PhD thesis, Library, Iowa State University of Science and Technology, Ames, 1965.
44. Roderick, G. L., and Demirel, T. Water Vapor-Sodium Montmorillonite Interaction. Highway Research Record 128, pp. 45-67, 1966.
45. Senich, D., Demirel, T., and Handy, R. L. Effect of Ca Montmorillonite Expansion on X-Ray Diffraction Intensities. Iowa State University of Science and Technology, Eng. Exp. Sta. Prog. Rept., 1966.
46. Topping, J. Errors of Observation and Their Treatment. The Institute of Physics, London, 1957.
47. Van Olphen, H. An Introduction to Clay Colloid Chemistry. Interscience Publishers, New York, 1963.
48. Van Olphen, H. Thermodynamics of Interlayer Adsorption of Water in Clays. I. Sodium Vermiculite. Jour. Colloid Sci., Vol. 20, pp. 822-837, 1965.
49. Wu, T. H. A Nuclear Magnetic Resonance Study of Water in Clay. Jour. Geophys. Res., Vol. 69, pp. 1083-1091, 1964.
50. Zettlemeyer, A. C., Young, C. J., and Chessick, J. J. Studies of the Surface Chemistry of Silicate Minerals. Jour. Phys. Chem., Vol. 59, pp. 962-966, 1955.